Western Washington University
Western CEDAR

Geology Graduate and Undergraduate Student Scholarship

Geology

10-2023

Using trace element concentrations in volcanic ash to elucidate magma sources to Koma Kulshan's (Mount Baker) most recent explosive eruption – the 6.7 ka BA (black ash) tephra

Stone Machel
Western Washington University, machels@wwu.edu

Follow this and additional works at: https://cedar.wwu.edu/geology_studentpubs

Part of the Geology Commons

Recommended Citation

Machel, Stone, "Using trace element concentrations in volcanic ash to elucidate magma sources to Koma Kulshan's (Mount Baker) most recent explosive eruption – the 6.7 ka BA (black ash) tephra" (2023). *Geology Graduate and Undergraduate Student Scholarship*. 5.
https://cedar.wwu.edu/geology_studentpubs/5

This Dissertation is brought to you for free and open access by the Geology at Western CEDAR. It has been accepted for inclusion in Geology Graduate and Undergraduate Student Scholarship by an authorized administrator of Western CEDAR. For more information, please contact westerncedar@wwu.edu.

Using trace element concentrations in volcanic ash to elucidate magma sources to Koma Kulshan's (Mount Baker) most recent explosive eruption – the 6.7 ka BA (black ash) tephra

Stone Machel
Advisor: Dr. Susan DeBari

Western Washington University
Department of Geology
Senior Thesis

Abstract

Koma Kulshan (Mount Baker) is an active stratovolcano in the northern Washington Cascades. Kulshan's most recent magmatic eruption at 6.7 ka was explosive, producing the ~0.2 km^3 BA tephra (black ash) from the edifice (Scott et al. 2019). Comprehensive geochemical data for the BA tephra were previously limited to major elements from one whole rock lapillus (silicic andesite) and several in situ glass analyses (dacite), despite being Kulshan's most voluminous Holocene tephra. Here, I present the first extensive major and trace element study of the pyroxene- and plagioclase-bearing BA tephra glass to determine magma source and eruption processes. My goal was to test whether the BA tephra magma was generated by rejuvenation of the source of the older, ~9.8 ka flank eruption that produced the 10-km-long zoned Sulphur Creek basalt/basaltic andesite lava flow. That zoned flow was derived from low-Mg basaltic magmas that mixed with a long-lived and laterally extensive upper crustal dacite mush (Garvey, 2022). I used 15 widely spaced BA tephra samples to first characterize the major and trace element variation of tephra glass (via SEM and LAICPMS) and compared those data with the silicic endmember of the Sulphur Creek lava flow. I found that the BA tephra glass is dacitic with little compositional variation (66-70% SiO_2), is high-K calc-alkaline, and has relatively steep REE patterns (La/Yb 8.5-11) with a strong negative Eu-anomaly. These characteristics and other trace element ratios such as Ba/La and Sr/Y suggest that the BA tephra is more closely related to Koma Kulshan's late Pleistocene H_2O-rich high-Mg basaltic andesite (HMBA) series than the low-Mg Holocene zoned lava flow. These results are important because they suggest that potentially explosive HMBA is the dominant magma composition that feeds the main Kulshan edifice, though it is not found in similar-aged flank eruptions. This suggests that two distinct but contemporaneous magma systems are feeding the volcanic field in close proximity.

Further work will use phenocryst barometry and phase equilibria to constrain the depth of the BA tephra magma source which is critical for interpreting subvolcanic architecture of the magmatic plumbing system.

Acknowledgements

I would like to take this page to recognize and thank everyone who made this project possible.

First off, I'd to give thanks to my advisor, Susan DeBari, for letting me be a part of this project. Sue's guidance and support throughout my senior thesis has helped to hone my scientific research skills. Her influence on my work has set me on the right foot for entering my geology career, which I'm so grateful for.

I'd like to thank Dave Tucker for his in the field guidance and generous sample donation. This project wouldn't have been possible without his knowledge of the Koma Kulshan Volcanic Field and his donation of samples. I'd also like to thank Doug Clark for donating a lake core sample during the project.

Thank you, Spencer Yaude and Clara Pfundt, for preparing the epoxy grain mount samples used in this study. Thank you to Mike Kraft for training me on the Tescan SEM. Thank you to Mai Sas for training and me on the LA-ICP-MS and guiding me through extensive data processing. Thank you to Kristina Walowski for guidance on sample preparations.

I'd also like to thank everyone part of the Evergreen State's Research in Volcanology and Petrology Team (ERVPT). Thank you for giving me a space to practice my igneous petrology skills and have intellectual discussions on my research.

Thank you to my family and friends for supporting my journey into geology.

While not directly funding my project, funding for the greater Koma Kulshan project was provided by the National Science Foundation (NSF).

Table of Contents

Abstract 1

Acknowledgements 3

Introduction 6

Geological Setting 8

Latest Pleistocene to Holocene Explosive Eruptions 9

Magma Series 11

Analytical Methods 13

Sample Collection and Preparation 13

TESCAN SEM Methods 15

LA-ICP-MS Methods 15

Comparing Major Element Concentrations Between SEM and LA-ICP-MS 16

Results 17

Whole Rock/Glass Composition 17

Major Elements 18

Trace Elements 19

REE Patterns 19

Interpretations 20

Unutilized Samples 20

Implications of Sourcing for BA tephra 22

Tephra Bulk Composition – Major Elements 22

Glass Spot Major Elements 22

Glass Spot Trace Elements 24

Implications 27

Conclusions 28

References 30

Tables 32

Figures 35

Appendices 50

Appendix 1: Major Element Concentrations Data table 50

Appendix 2: Trace Element Concentrations Data table 61

Introduction

Koma Kulshan (Mount Baker) is the northernmost Cascade Arc volcano in the United States Pacific Northwest. The Cascade volcanic arc extends from southwestern British Columbia through Western Washington, Oregon, and into Northern California. Koma Kulshan is an andesitic stratovolcano that is second to Mount Rainier as the most glaciated volcano in the United States (Figure 1).

The most recent magmatic explosive eruption from Koma Kulshan was at 6.7 ka, erupted from Sherman Crater, producing a tephra couplet of the OP (phreatic) and the BA (magmatic) tephra (Scott et al., 2020). Current exposures of the BA tephra are in an elliptical isopach that is extended to the northeast at ~33 km from the volcano (Figure 2). The eruption of the BA tephra is the largest magnitude Holocene eruption from Koma Kulshan. However, the eruption itself is estimated as a tenth of the magnitude of the 1980 Mt. St. Helens eruption (Scott et al., 2020). There are limited geochemical analyses of the BA tephra (Black-Andesite) (Scott et al., 2020). With this, there are no conceptual models of the BA tephra's magma sourcing or the depth of its magma chamber. This study presents the first geochemical characterization of the BA tephra and tests hypotheses for its magma sourcing and drivers of eruption.

This study contains the first comprehensive geochemical analyses of the major and trace elements of Tephra Layer BA. These analyses are critical in understanding the magma sourcing for Koma Kulshan because this volcano has erupted distinct magma types from four different magma families (e.g., Moore et al., 2012). Each of these families is indicative of different magma ascent processes and is ultimately derived from different sub-Moho sources (Moore et al., 2012; Sas et al., 2017). The eruption of the BA tephra has not yet been characterized as belonging to any of these given magma families. Two of these magma families, an alkaline

series and a low-K olivine tholeiite (LKOT) series, are unlikely to have sourced the BA tephra eruption as there is no record of eruptions of these two magma compositions in the Holocene (Scott et al., 2020) and they occurred rarely throughout the Late Pleistocene. However, the other two series of calc-alkaline magmas are primary contenders for sourcing the BA tephra as there have been Holocene eruptions of their composition. These two primary magma families are 1) the low-Mg calc-alkaline magma series and 2) high-Mg (HMA/HMBA) magma series. The low-Mg calc-alkaline series most recently erupted during magma rejuvenation of a dacitic mush by injection of low-Mg basalt (Garvey, 2022). This initiated the eruption of the zoned Sulphur Creek lava flow at ~9.8 ka, that is basalt at the toe and basaltic andesite further up the source cone (Schreiber's Meadow Cinder Cone). The most HMA/HMBA series erupted as multiple lava flows late-Pleistocene to as young as 14 ± 9 Ka (Glacier Creek Andesite) (Baggerman et al., 2011; Gross, 2012; Escobar et al., 2017).

The goal is to test the hypothesis that the BA tephra derived from the same primitive magma series as the Sulphur Creek lava flow, the low-Mg calc-alkaline basalt that caused dacitic remobilization in the Holocene (Garvey, 2022). This hypothesis is attributed to the glass shards of the BA tephra being dacitic in composition. The Sulphur creek lava flow is also the second most recent magmatic eruption before the eruption of the BA tephra, which leaves speculation for another mush remobilization in that span of time between 9.8-6.7 ka. This study presents detailed geochemical analyses of glass shards in the BA tephra, including major element and trace element chemistry of these glass shards.

Geological Setting

The Cascade Arc extends 1250 km from Lassen Peak in northern California to Mount Meager in southern British Columbia along the west coast of North America (Hildreth et al., 2007). The subduction of the Juan de Fuca plate eastward underneath the North American plate initiates Cascadian arc volcanism with a variable convergence rate (Figure 1). The top of the subducting Juan de Fuca plate underneath Koma Kulshan is ~90-100 km deep (McCrory et al., 2004), with an estimated age of 19-20 Ma (Green et al., 1999). The basement rocks of this subducting crust are composed of Mesozoic and Paleozoic rocks of several tectonic terranes (Hildreth et al., 2003) that were accreted during the Cretaceous and redistributed by extensional and strike-slip faulting in the Paleogene (Misch, 1966; Brown, 1987; Tabor et al., 2003).

Koma Kulshan (3286 m) is primarily an andesitic stratovolcano that is the northernmost Cascade Arc volcano in the United States (Scott et al., 2020). It is the youngest volcano of a 1.3-million-year-old active volcanic field (Scott et al., 2020). The Koma Kulshan volcanic field has evolved over its continuously active timeline. The super-eruption and collapse of the Kulshan Caldera (1.15 Ma) released 50 km^3 of dominantly rhyodacitic magma, presumably leaving solidified remnants of its magma chamber in the crust beneath the northern flanks of Koma Kulshan. The scale of this eruption is comparable to the Holocene eruption of Mount Mazama in Oregon, forming the Crater Lake Caldera (Bacon et al., 1983). After the caldera collapse, mostly andesitic activity continued Kulshan caldera edifice (0.9-0.5 Ma). Formation of the primarily andesitic Black Buttes stratovolcano began after the Kulshan Caldera collapse 0.5-0.2 Ma. The construction of the current Koma Kulshan edifice formed 50-10 ka off the east flank of the now eroded and extinct Black Buttes (Hildreth et al., 2003). Off the south side of Koma Kulshan, the Schreiber's Meadow Cinder Cone formed during the eruption of the Sulphur Creek ~9.8 ka.

Latest Pleistocene to Holocene Explosive Eruptions

Pre-Holocene eruptions from Koma Kulshan include lava flows and minor pyroclastic flows, but no airfall tephras are preserved due to the melting of glacier ice that removed those deposits. Latest Pleistocene to Holocene eruption deposits from Koma Kulshan have included small to moderate volume tephra deposits, and summit and off-flank lava flows. Latest Pleistocene and earliest Holocene tephra deposits are sourced from the Carmelo Crater summit vent. Holocene tephra deposits have been sourced from peripheral vents, including Sherman Crater and Schreiber's Meadow Cinder Cone. The Late Pleistocene to present stratigraphic record around Koma Kulshan includes 6 tephra layers produced by explosive eruptions, three of which are phreatic and 3 of which are magmatic: Tephra Sets SP and SC (magmatic), Tephra layer MY (phreatic), Tephra Set OP (phreatic), Tephra Layer BA (magmatic), and Tephra Set YP (phreatic), from oldest to youngest. Tephra sets and tephra layers differ, where a tephra set comprises multiple layers of tephra that represent a discrete depositional unit with distinct stratigraphy, whereas a tephra layer is, as the name implies, just one layer. Tephra is easily erosive and granular, so these Holocene tephra outcrops have experienced some remobilization.

Tephra Set SP (~12.7 ka) is identified as andesitic ash, with fine-sand sized pyroclastics and enigmatic scoria is exposed along the top of Grant Peak (Scott et al., 2020). The tephra set erupted from the main Koma Kulshan edifice of Carmelo Crater, depositing in 2 pulses: silty soil with vitric andesite ash followed by the SP tephra. The SP tephra is dark gray to black in color. It is the oldest known post-glacial tephra deposit that shows up in the KKVF stratigraphic record. At the time of eruption, no evidence suggests the existence of the Sherman Crater vent (Scott et al., 2020).

Tephra Set SC (~9.8 ka) is identified as a basaltic ash and lapilli. The eruption of this set sourced from the Schreiber's Meadow cinder cone (Figure 3). The main layers of the set are black to oxidized orange lithic ash and scoriaceous basaltic lapilli, with interbedded secondary layers of fine-grained basaltic ash. The set has an overall distinctive orangish-reddish brown color. The distribution of this main layer deposit includes scoria lapilli 4 km northeast from the source vent, and ash 20 km in the same direction. Minor layers of the SC set include fine-grained ash columns (Scott et al., 2020). The Tephra Set SC overlies the Sulphur Creek basalt lava flow (~9.8 ka), also sourcing from the Schreiber's Meadow Cinder Cone (Scott et al., 2020; Figure 3).

Tephra Layer BA (~6.7 ka) is identified as andesitic ash and lapilli. It is the only known magmatic eruption sourced from the Sherman Crater edifice during the Holocene. The tephra is fully to partially composed of glassy clasts containing phenocryst assemblage of plagioclase, clinopyroxene, orthopyroxene, and oxide minerals, from greatest to least abundance, respectively. The BA tephra has a silicic andesitic bulk composition (~62 wt.% SiO_2), with the glass matrix of the BA tephra being dacitic in composition (~67.5-68.5 wt.%), based on only a few major element analyses (Scott et al., 2020). The eruption of the BA tephra produced 0.1 km^3 of ash, making it the most voluminous remaining tephras in the volcanic field. Deposits of the BA tephra are found within elongate ellipsoidal isopachs that extend ~33 km northeast from Koma Kulshan (Figure 1). However, as the Tephra layer BA is loose and granular, remobilization of these deposits due to glaciation is inevitable. Within the OP tephra couplet, the BA tephra and OP tephra interbeds are found in local outcrops, suggesting alternating periods of phreatic and magmatic activity (Scott et al., 2020).

There is uncertainty in the utilized samples being BA tephra, as tephra sample age constraints aren't perfect. Deposits of the SC, SP, and BA tephra are located through rough

terrane, influencing mixing and mobilization of tephra layers/sets. There may also be smaller/thinner tephra layers/sets that haven't been recorded yet in the KKVF stratigraphic record. Given this, samples obtained and considered as BA tephra may be of a different tephra unit, which is discussed amongst specific samples later in the paper.

Magma Series

The Koma Kulshan Volcanic field (KKVF) is represented by four geochemically distinct parental magma sources in the trans-crustal magma system. These endmembers sources include a low-K olivine tholeiitic (LKOT) series, an alkaline series, a low-Mg calc-alkaline series, and a high-Mg calc-alkaline andesite/basaltic andesite (HMA or HMBA) series. Each of these magma series are geochemically distinct from one another.

The LKOT series within the KKVF displays some geochemical characteristics that are similar to mid ocean ridge basalts as indicated by the ~716 ka Park Butte basaltic lava flow. However, the Park Butte unit outcrops 7.5 km off the southwest flank of Koma Kulshan (Moore et al., 2012). The Park Butte unit shows a similar major element chemistry to other LKOT-derived units erupted along the Cascade Volcanic Arc. REE patterns of the Park Butte unit have a plateau trend that are representative of MORB-like patterns, with depletions in Nb, Ta, Zr, and mid-REEs (Sm, Eu), compared to other eruptive units within the KKVF (Moore et al., 2012).

The Alkaline series is distinguished by its high-K concentrations, indicative of deep mantle partitioning and deeper magma generation (such as hotspot settings). The Alkaline series of the KKVF is represented by the Coleman Pinnacle Andesite (~305 ka) and the Nooksack Falls dacite (~149 ka) (Escobar, 2017; Gross, 2012). Samples from both units plot in the alkaline field with higher concentrations of alkali oxides, ranging in composition from trachyandesite to

trachydacite to dacite (Escobar, 2017; Gross, 2012). REE patterns of Nooksack falls display a slightly steeper slope trend (La/Yb = 7.4-7.7) than to other KKVF units (Gross, 2012), while REE patterns of Coleman Pinnacle are even steeper in slope trend (La/Yb = 10-24) (Escobar, 2017). This difference between the REE patterns of these alkaline derived units is correlated to magma composition, as Coleman Pinnacle is andesitic, and Nooksack Falls is dacitic.

The low-Mg calc-alkaline series is typical of arc magmas worldwide, represented in the KKVF by the Lake Shannon basalt (~94 ka) and the Sulphur Creek basalt (~9.8 ka). Bulk compositions of units derived from the low-Mg calc-alkaline series range from basalt to basaltic andesite (Moore et al., 2012). The Lake Shannon and Sulphur Creek units show diagnostic enrichments in large ion lithophile elements (Ba, Rb, K, Pb), also exhibiting higher abundances of Nb, Ta, Zr, compared to other KKVF units (Moore et al., 2012). REE patterns of Sulphur Creek lavas are distinctive from other KKVF units from their enrichments in HREEs (Dy, Ho, E r, Tm, Yb, Lu), and have a moderate average REE slope trend (La/Yb = 5.7) (see later discussion).

The HMA/HMBA series of the KKVF is typical of arc magmas, compared to the LKOT and alkaline series, with a defining Mg-enrichment and moderate K concentrations (Escobar, 2017). This is a common magma type erupted from Cascade arc volcanoes (Grove et al., 2005). The HMA/HMBA is the most common magma series erupted in the KKVF, and the two most recent eruptions that are part of this series are the Swift Creek basaltic andesite (~48 ka) and the Glacier Creek (~14 ka) basalt. Bulk compositions of HMA/HMBA series generally range from rhyolites to basalts in SiO_2 wt. % (Baggerman et al., 2011; Gross, 2012; Moore et al., 2012; Escobar, 2017). Units derived from the HMA/HMBA series have moderate average REE slope

trend (La/Yb = 8.52), which is steeper in comparison to units derived from the low-Mg calc-alkaline series (La/Yb = 5.70) (see later discussion).

In considering magma sourcing for the BA tephra, I've compared my results to geochemical data from HMA/HMBA series (Baggerman et al., 2011; Gross, 2012; Moore et al., 2012; Escobar, 2017) and low-Mg calc-alkaline series (Moore et al., 2012; Garvey, 2022) eruptive units. Eruptive units derived from the LKOT and the alkaline series are anomalies in the KKVF eruptive history, given they are so geochemically distinct from typical arc setting primitive magmas. The HMA/HMBA and low-Mg calc-alkaline series, on the other hand, are typical and more representative of arc setting primitive magmas. The HMA/HMBA series is the most prominent magma type erupted in the KKVF, and Escobar and DeBari (2021) link these to deeper crust high-Mg primitive basalts. The low-Mg calc-alkaline series sourced the second most recent magmatic eruption from the KKVF (the Sulphur Creek lava flow at ~9.8 ka), through a proposed dacitic remobilization (Garvey, 2022). Initial comparison of the LKOT series and alkaline series shows they are not at all similar to pre-existing BA tephra glass data, so they are removed from consideration.

Analytical Methods

Sample Collection and Preparation

13 of the 15 tephra samples were provided and generously donated by Dave Tucker, a research associate in the Geology Department of Western Washington University. His samples are denoted with a "DT" followed by the date of collection, from 1997 to 2020. The samples with this notation include DT090797 (Glacier Creek), DT081105C (Park Butte), DT082005A (Shuksan Lake Trail), DT062506 (Gold Run Pass Trail), DT072306B (Heliotrope Trail),

DT092706C (Boulder Ridge), DT070607A (Schriebers Meadow Road), DT091407A (Cow Heaven Trail), DT072609 (Ptarmigan Ridge), DT091109 (Thunder Lakes), DT091409A (Spoon Lake), and DT080920 (Damfino Lake Trail), from oldest to most recent collection, respectively. Additionally, a sample utilized of Tucker's collections is labeled "BA near Sherman". 1 of the 15 samples was obtained from a Heathers meadows lake core by Dr. Doug Clark of Western Washington University, circa 1997, labeled as HLGPush1_BA. The last of the 15 samples was collected in September 2022, in the tephrostratigraphy along the Scott Paul Trail, where the sample is labeled 22kk-BAt-02b.

All tephra samples were prepared in epoxy grain mounts at Western Washington university. All epoxy grain mounts used in the study were prepared by Spencer Yaude, apart from HLGPush_BA, prepared by WWU undergraduate Clara Pfundt. To prepare an epoxy grain mount, an empty circular plastic tube is taped with doubled-sided tape and adhered to a glass plate. A small scoop of each sample was put on the tape at the bottom of the mount to produce a thin layer of tephra. Epoxy is prepared using 100 parts resin to 45 parts hardener. This epoxy mixture is added to each of the tephra-lined mounts to produce a thin layer. Once the epoxy mixture is set, the mounts are set in a vacuum chamber to dry and cure for 24 hours. After this period, the double-sided tape is removed to expose the bottom of the mount. Each mount was polished using 220 grit silicon carbide paper, followed by 500 grit, followed by 800 grit, then finally with 1 μm diamond grit past for polishing.

TESCAN SEM Methods

Major element concentrations of glass spots were analyzed at Western Washington University (WWU) on a Tescan Vega 3 Thermionic Scanning Electron Microscope (SEM) with an 80 mm^2 Oxford energy dispersive X-max energy dispersive spectrometer (EDS) enabled. All epoxy mounts were prepared using a carbon coater with an ~30 nm thick coating. Constant SEM parameters for each sample analysis include a working distance of 15 mm, accelerating voltage of 20kV, EDS process time of 4, detector dead time of ~40-50% during spectral acquisition, and a drop count rate of $2x10^5$ counts. A beam intensity of 17 was used in measuring characteristics of different major elements with the EDS detector, which also aided in visualizing glass spots on the SEM. The oxides analyzed for each glass spot include SiO_2, TiO_2, Al_2O_3, FeO, MnO, MgO, CaO, Na_2O, K_2O, and P_2O_5.

EDS spectra were obtained from different points within the confines defined parallelograms within chosen glass fragments. I set these parallelograms to have length and width axes no smaller than ~30-50 μm (Figure 4), with some as large as ~160 μm. 212 glass spectrum analyses were made, with a total of 39 glass spots analyzed. Brightness and contrast were utilized in deciphering glass from microlites and other plagioclases. Each epoxy mount had constant scale for: $2x10^4$ μm, 6000 μm, 1000 μm, and 200 μm for analyzed glass spot (Figure 4). All images had a live frame accumulation of 2, and an acquisition of 22-45 seconds.

LA-ICP-MS Methods

Major and trace element concentrations of glass were analyzed by laser ablation inductively coupled plasma mass spectroscopy (LA-ICP-MS) at WWU using an Applied Spectra RESOlution-SE 193 nm laser ablation system coupled to an Agilent 7900 ICP-MS. Analyses of

glass occurred on the same locations as on the SEM. Glass spots were analyzed over the course of two sessions using a 30 μm diameter beam with fluence of 1.68 J/cm^2 and a 10 Hz repetition rate. Each spot analysis was run in 30 second intervals. The carrier gas was He with a flowrate set at 400 mL/minute, mixed with 5mL/minute of N_2 to improve sensitivity. An NIST 610 glass was used for instrument tuning. The oxide ratio was monitored using $^{248}ThO/^{232}Th$ (<0.151%) and the doubly charged ratio was monitored using $^{22}Ca^{2+}/^{44}Ca^{+}$ (<0.154%).

USGS glass standard GSD-1G (n=15) was used as an external standard and ^{27}Al was used as an internal standard (Table 1; Jochum et al., 2005). The elements analyzed include ^{23}Na, ^{25}Mg, ^{27}Al, ^{29}Si, ^{39}K, ^{43}Ca, ^{45}Sc, ^{47}Ti, ^{57}Fe, ^{60}Ni, ^{85}Rb, ^{88}Sr, ^{89}Y, ^{90}Zr, ^{93}Nb, ^{133}Cs, ^{137}Ba, ^{139}La, ^{140}Ce, ^{141}Pr, ^{146}Nd, ^{147}Sm, ^{153}Eu, ^{157}Gd, ^{159}Tb, ^{163}Dy, ^{165}Ho, ^{166}Er, ^{169}Tm, ^{171}Yb, ^{175}Lu, ^{178}Hf, ^{181}Ta, ^{206}Pb, ^{207}Pb, ^{208}Pb, ^{232}Th, and ^{238}U with 2sd precision of 1-6%. USGS glass standards GSE-1G and BHVO-2G (n=15) were used as secondary standards to monitor precision in results, and their analyzed elemental abundances were consistent with values previously reported (Table 2 & 3; Jochum et al., 2005). Data processing of each sample was done using GLITTER (Griffin et al., 2008). Samples were labeled in correlation to the epoxy mount classification: mount-circle-grain_sample.

Comparing Major Element Concentrations Between SEM and LA-ICP-MS

Major element concentrations were obtained both by SEM and LA-ICP-MS. Figure 5 displays a comparison between these analyses after converting LA-ICP-MS data from ppm element to wt.% oxides. For concentration collections to be accurate, data should yield a positive linear array with a slope of ~1.

The only plot that shows a linear relationship is Al_2O_3, which is expected, given that SEM Al_2O_3 values were used as an internal standard for ^{27}Al (Figure 6b). The rest of the compared major element oxides are scattered and non-linear. Na_2O concentrations plot lower on the SEM than the LA-ICP-MS, which may be caused by volatile loss on the SEM. SEM major element concentrations were represented in my results, as sample count frequency is higher for dacitic glass shards (~63-70 wt.% SiO_2). CaO concentrations plot as a roughly linear relationship, even though concentrations obtained on the SEM are lower. FeO, K_2O, and TiO_2 concentrations show no trend at all, plotting as a scatter. Both SiO_2 and MgO concentrations plot along a roughly horizontal trend. However, SiO_2 and MgO concentrations from the LA-ICP-MS show a much wider variation than those from the SEM (SiO_2 distributions represented in Figure 5). For this reason, major element concentrations obtained from the SEM are represented in the results.

Results

Whole Rock/Glass Composition

Results for major element contents in the BA tephra glass are reported in Appendix 1. Distribution of SiO_2 concentrations in BA tephra glass spots is shown in a histogram in Figure 5a. Glass analyses are dacitic, ranging from 63 to 72 wt.% SiO_2, with most glass spots within 66-70 wt.% SiO_2. The highest frequency of analyses (11 spots) contains 66-68 wt.% SiO_2 (Figure 5a). Figure 7 displays the BA tephra glass analyses on a Total Alkali vs Silica diagram (TAS) along with whole rock analyses of lava flows from different KKVF magma series. Most lava samples span the basalt-andesite-dacite field or are on the boundary with trachybasalt, basaltic

trachyandesite, trachyandesite-trachydacite. The BA tephra glass compositions plot in the trachydacite-rhyolite or dacite-rhyolite field.

Two clusters of BA tephra glass spot samples are visible in Figures 7 and 8. One cluster, encapsulating most BA tephra glass analyses, plots between 63-71% SiO_2 whereas another smaller cluster plots at ~78% SiO_2. Field notes from D. Tucker (personal communication) show that these higher SiO_2 samples are not actually BA tephra and are likely not native to Koma Kulshan. They will not be discussed further in this thesis.

HMA/HMBA and low-Mg series lavas (whole rock data) from Koma Kulshan are plotted for comparison plot along a similar array on the TAS diagram (Figure 7), although the low-Mg series appears to plot at higher alkali concentrations for a given SiO_2 content. BA tephra glass samples generally plot in a cluster at higher SiO_2 concentrations than these bulk rock data and are also higher in alkalis. The bulk lavas plot in the moderate-K calc-alkaline field in Figure 8. Some HMA/HMBA samples straddle the dividing line between the moderate-K and high-K calc-alkaline series. Many of the BA tephra samples plot in the high-K calc-alkaline affinity field, following a trend from the most Si-rich HMA/HMBA to higher K_2O concentrations (>3 wt.% K_2O) (Figure 8). LKOT basalt samples cluster at low SiO_2 and low alkali oxide concentrations (Figure 7) and the moderate-K calc-alkaline affinity field in Figure 8. The alkaline series plots as a horizontal array in the trachyandesite to trachydacite field in Figure 7 and in the high-K calc-alkaline field in Figure 8.

Major Elements

BA tephra glass analyses and representative lava bulk compositions from previous work are plotted on major element Harker diagrams in Figure 9. Also plotted is one BA tephra bulk composition (via XRF) from a lapillus sampled near Sherman Crater (Hildreth et al., 2003; Scott

et al., 2020). This BA tephra bulk composition plots within the array of the HMA/HMBA series and the low-Mg calc-alkaline series in Figure 9. However, the composition of the BA tephra lapillus has lower Na_2O and TiO_2 than the low-Mg calcalkaine series.

BA tephra glass data shows a clear extension of thee HMA/HMBA trend in Figure 9 except for very scattered Na_2O data (likely due to Na migration under the beam on the SEM). In Figure 9f, TiO_2 concentrations in the BA tephra glass show scatter, likely related to the presence of Fe-Ti microlites.

Trace Elements

Trace element concentrations in the BA tephra glass are reported in Appendix 2, including reported trace element concentrations for standards analyzed as unknowns. Error between analyses of standards as unknowns and reported values is <5%.

BA tephra glass samples and representative bulk compositions from the HMA/HMBA series and the low-Mg calc-alkaline series are plotted on trace element Harker diagrams (Figure 10). BA tephra glass data generally plot at the end of the HMA/HMBA and low-Mg calc-alkaline series arrays (e.g., Ba, Th in Figure 10e, f). Some BA tephra glass trace element data shows clear extensions of just the HMA/HMBA series (Sr, Y, Zr, and Yb in Figures 10a, b, c, & g).

REE Patterns

REE element spider diagrams of BA Tephra glass data compared to the HMA/HMBA series and low-Mg calc-alkaline series bulk composition data are displayed in Figure 11. Each line represents one sample data point.

Primitive mantle normalized, extended REE diagrams of representative BA Tephra glass samples are reported along with representative HMA/HMBA series samples (in Figure 11a) and

with representative low-Mg calc-alkaline samples (in Figure 11c). In Figure 11a, the BA tephra glass shows similar enrichments in U, K, and Pb, with similar depletions in Nb, Ta, La, Ce, and Ti, compared to the HMA/HMBA series. In Figure 11c, the BA Tephra glass shows similar enrichments in U, K, and Pb, with similar depletions in Nb, Ta, La, and Ce, compared to the low-Mg series.

Chondrite normalized REE diagrams of representative BA Tephra glass samples are reported along with representative HMA/HMBA series samples (in Figure 11b) and with representative low-Mg calc-alkaline samples (in Figure 11c). Eu-depletion in BA Tephra samples is attributed to samples being glass from which plagioclase has been extracted (e.g., plagioclase microlite crystallization, which are abundant) (Figure 11b & d). There is no Eu-depletion in the HMA/HMBA and low-Mg calc-alkaline samples, presumably because of limited plagioclase extraction (Figure 11b & d). While the REE slope trends of the HMA/HMBA series and the low-Mg calc-alkaline series are similar to the BA Tephra, the HMA/HMBA series displays a greater depletion in HREEs than the low-Mg calc-alkaline series, yielding higher La/Yb ratios (Figure 11b & d). The HMA/HMBA series and low-Mg calc-alkaline series have similar enrichments of LREE (Figure (11b & d) that are lower than the BA tephra.

Interpretations

Unutilized Samples

As discussed earlier, misidentification of some tephra samples requires removal from consideration as representing the BA Tephra glass shard geochemistry. These samples are as follows: DT091407A, DT090797 (=MB578), DT081105C, DT072609 (from GM 2, circle 5), DT091409A, and DT072306B (from GM 16, circle 3) (see Appendix 1). The analysis of these

unutilized samples can be attributed to mislabeling of samples in preparation and/or collection. These samples are not plotted in Figures 9-14.

DT091407A, DT081105C, DT091409A, and DT072609 (GM 2, circle 5) are high-Si rhyolite composition (~77-79 wt.% SiO2) (Figure 7) whereas most BA Tephra glass samples are trachytic in composition (~63-70 wt.% SiO_2) (Figure 7). Alkali oxide concentrations for these samples are moderate (~6.5-7.5 wt.% $Na_2O + K_2O$), compared to most BA tephra having much higher concentrations (~7-9.5 wt.% $Na_2O + K_2O$) (Figure 7). The average La/Yb ratio for DT091407A is ~14.05, for DT081105C is 15.36, for DT091409A is 13.34, and DT072609 (GM 2, circle 5) is 19.36. which is much higher than average La/Yb ratio for the BA Tephra (Appendix 2, and Figure 11b & d). The higher SiO_2 concentrations and La/Yb ratio in these samples indicate that they're not from the Tephra Layer BA and were sampled from some other tephra unit in the field. The higher La/Yb ratios from these samples suggests different volcanic sources than any of the magma series in the KKVF (Figure 11b & d).

DT090797 (=MB578) is andesitic in composition, with a 62.79 wt.% SiO_2 (Figure 7 & 8, and Appendix 1). While this is a lower SiO_2 concentration than expected in a BA Tephra glass sample, the REE chemistry in DT090797 is also indicative of sourcing from the HMA/HMBA series. The La/Yb ratio reported for DT090797 is 8.50 and the average La/Yb ratio of the HMA/HMBA series is ~8.52 (Appendix and Figure 11b). Given a different SiO_2 content but a similar La/Yb ratio to KKVF sourcing, the origin of DT090797 is enigmatic.

DT072306B (from GM 16, circle 3) is Eu-enriched, while other DT072306B samples have an Eu-depletion (Appendix 2). This Eu-enrichment is indicative of a plagioclase-enriched glass spot. Eu^{2+} partitions into Ca-rich plagioclase (anorthite) in replacement of Ca^{2+}, as both elements have the same charge and atomic radii. In typical volcanic glass, Eu is, given that most

Eu^{2+} has partitioned into plagioclase that has left the melt. Since the glass spot analyzed in DT072306B (from GM 16, circle 3) was Eu-enriched, it is likely that the LA-ICP-MS ablated a plagioclase microlite rich glass shard. DT072306B (from GM 16, circle 3) is therefore not representative of the BA Tephra glass trace element chemistry.

Implications of Sourcing for BA tephra

Tephra Bulk Composition – Major Elements

Major element compositions of the bulk BA Tephra and glass display similar trends to the HMA/HMBA series and low-Mg calc-alkaline series (Figure 9). Bulk composition of the BA tephra (from Hildreth et al., 2003, XRF lapillus analysis) (Appendix 1), plots within array of both series in Figure 9.

There is no clear association of major elements in the BA Tephra bulk composition with either the low- or high-Mg calc-alkaline magma series, although its SiO_2 content is on the high end of the low-Mg series (Figure 9). The two exceptions are Na_2O and TiO_2, where the BA Tephra bulk composition plots within the HMA/HMBA series (Figure 9d). While this can indicate similar sourcing of these major element oxides with the BA Tephra, it's not sufficient to geochemically distinct a possible magma source. If the tephra is variable in composition, more bulk composition data points might better associate BA Tephra with either of the calc-alkaline series.

Glass Spot Major Elements

Major element concentrations in BA Tephra glass plot in a similar array to the HMA/HMBA series and the low-Mg calc-alkaline series. Given that the BA tephra samples are of glass composition as opposed to bulk composition, they report at higher, more felsic SiO_2

concentrations (~65-72 wt.% SiO_2) (Figure 9). With higher SiO_2 contents and plotting along similar array to the calc-alkaline series, BA Tephra glass samples represent the highest enrichments and depletions in major elements compared to calc-alkaline magmas erupted in the KKVF. This is because the volcanic glass matrices of tephra are representative of a quenched magma.

Concentrations of Al_2O_3, FeO, CaO, and MgO decrease in the trend from bulk rock analyses to BA tephra glass as SiO_2 increases (Figure 9a-c, & g). Increase in these major element oxides is indicative of mafic minerals crystallizing and partitioning out of the melt as SiO_2 increases. This leaves the BA Tephra glass depleted in mafic elements, and more enriched in felsic elements, such as Na and K.

Concentrations of K_2O increase in the trend from bulk rock analyses to BA tephra glass as SiO_2 increases (Figure 9e). However, there is no clear trend in Na_2O content given the wide range from ~3-6 wt.% (Figure 9d). The scattered Na_2O concentrations data from the glass can be attributed to inaccurate measurements on the SEM. The Tescan SEM at WWU had been experiencing problems with Na readings at the time frame of this study, where Na plots at a much higher concentration than expected. When comparing Na_2O concentrations take from the SEM and the LA-ICP-MS, there was also clear trend (Figure 5).

Concentrations of TiO_2 in the BA Tephra glass show scatter, likely due to inadvertent analysis of Fe-Ti oxide microlites (Figure 9f).

The BA Tephra glass follows the main trend of the HMA/HMBA series and clusters at Mg# =~15-35 at the bottom of the array (Figure 9h). The Mg# ratio in the HMA/HMBA series sharply decreases as SiO_2 increases, where the low-Mg calc-alkaline series plateaus at higher Mg# ratios (~49-58) as SiO_2 increases.

Most of the BA Tephra glass major element contents plot along a similar array to both KKVF calc-alkaline series (Figure 9). This suggests the BA Tephra glass was indeed sourced from a calc-alkaline magma source. To better discern similarity in glass composition from the BA Tephra to either of the calc-alkaline series, groundmass glass compositions from the HMA/HMBA and low-Mg eruptive units are discussed below.

Glass Spot Trace Elements

Trace element compositions of the BA Tephra glass fall along a similar array as both KKVF calc-alkaline series (Figure 10). However, some trace element trends are more clearly linked to the HMA/HMBA series. Many incompatible trace elements that partition almost exclusively into the residual melt liquid that is quenched in eruption are used as fingerprints for magma sourcing. Trace element data helps to compare specific enrichments and depletions that are characteristic of the BA Tephra glass, the HMA/HMBA series, and the low-Mg calc-alkaline series.

Concentrations of Sr in the BA Tephra glass are depleted, following a trend of steeply decreasing Sr as SiO_2 content increases in the HMA/HMBA series (Figure 10a, and Figure 11a & c). BA Tephra glass samples cluster at lower Sr values, indicative of Sr partitioning into anorthite (Ca-rich plagioclase) during fractional crystallization and out of the residual melt (Figure 10a). This makes sense, as quenched magma preserves the residual melt without a phenocryst assemblage, so Sr decreasing in the glass represents a decrease in plagioclase. BA Tephra glass samples that plot at higher Sr concentrations (and Al_2O_3) than the bulk cluster of reported data is likely due to microlite plagioclase being ablated during LA-ICP-MS analyses

(e.g., HLGPush1). There is no clear similarity in Sr content between the BA Tephra glass and the low-Mg calc-alkaline series trend which plateaus with increasing SiO_2 (Figure 10a).

Concentrations of Y vs. SiO_2 in the BA Tephra glass plot at the end of the increasing array of the HMA/HMBA series (Figure 10b). The low-Mg calc-alkaline series gently decreases in Y contents as SiO_2 increases, opposite of the BA Tephra glass and HMA/HMBA data. This suggests the BA Tephra glass contains similar enrichments in Y to the HMA/HMBA series.

BA Tephra glass clusters at high-Zr concentrations as a cluster, compared to the lower-Zr array of the KKVF calc-alkaline series (Figure 10c, and Figure 11a & c). However, this cluster plots within similar array of the HMA/HMBA series (Figure 10c). The HMA/HMBA series increases gently in Zr as SiO_2 increases. In contrast, the low-Mg calc-alkaline series plateaus or slightly decreases in Zr content as SiO_2 increases (Figure 10c). While it's true that the BA Tephra glass aligns with the HMA/HMBA series array, its Zr concentrations are much higher. This could be due to Zr partitioning into HMA/HMBA residual melt and not into mineral assemblages during fractional crystallization.

BA Tephra glass plot as a La-enriched cluster in Figure 10f. The cluster plots in the HMA/HMBA series array, where HMA/HMBA increases in La content while SiO_2 increases (Figure 10f). BA Tephra and HMA/HMBA samples plot within a same array (~24-32 ppm La and ~65-68 wt.% SiO_2) (Figure 10f). This suggests that the BA Tephra contains similar enrichments in La to the HMA/HMBA series.

BA Tephra glass plots at high Ba concentrations (~775-1550 ppm), similarly to a cluster of HMA/HMBA dacites (~900-1000 ppm) (Figure 10e). The BA Tephra glass cluster plots along a similar array to the HMA/HMBA series, where Ba contents increase with SiO_2 increase. Similarly, the low-Mg calc-alkaline series increases in Ba with increase in SiO_2. It's more

plausible that the Ba concentrations in the BA Tephra glass are along the similar array of the HMA/HMBA series, as HMA/HMBA samples are reported within the cluster of BA Tephra glass data. This suggests that the BA Tephra glass contains similar enrichments in Ba to the HMA/HMBA series.

Concentrations of Th in BA Tephra glass plot along similar array to both KKVF calc-alkaline series (Figure 10h). Both the HMA/HMBA series and the low-Mg calc-alkaline series moderately increase is Th as SiO_2 increases. Given that both the HMA/HMBA series and the low-Mg calc-alkaline series plot along a similar array (Figure 10h), it's sufficient to suggest that the BA Tephra contains similar enrichments of Th to KKVF calc-alkaline magmas.

The BA Tephra glass plots along the same Yb vs. SiO_2 array as the HMA/HMBA series (Figure 10g). Concentrations of Yb in increase steeply with SiO_2 in the HMA/HMBA series array and slightly overlap with the BA tephra glasses (Figure 10g). This suggests that the BA Tephra contains similar enrichments in Yb to the HMA/HMBA series.

La/Yb ratios acts as a proxy for averaging the REE pattern slope trend (Figure 12). The average REE slope trend for the BA tephra is La/Yb ~ 9.6 (Figure 12). For the HMA/HMBA series La/Yb is ~ 8.5 (Figure 11b, Figure 12), and for the low-Mg calc-alkaline series La/Yb is ~ 5.7 (Figure 11a, Figure 12. The La/Yb ratio for the BA Tephra is more like the HMA/HMBA series, with the low-Mg series having a shallower average REE slope. Average La/Yb ratios for BA tephra were calculated using data reported in Appendix 2. As seen in Figure 12, the range of BA Tephra La/Yb ratios is ~8-11 overlapping with the HMA/HMBA series (~6.75-11.75), but the low-Mg calc-alkaline series is lower (~4-7). This indicates that BA Tephra sourced from a similar magma series as the HMA/HMBA series.

The Ba/La ratio of BA Tephra glass overlaps with that of the HMA/HMBA series (Figure 13). The Ba/La ratio for the BA Tephra ranges from ~22-35, whereas the ratio for the HMA/HMBA series ranges from ~20-46. Plotting Ba/La vs La/Yb, the BA Tephra and the HMA/HMBA series both cluster at high Ba/La and La/Yb ratios. On the opposite end, the low-Mg calc-alkaline series plots at lower Ba/La (~16-23) and lower La/Yb ratios (~4-7) (Figure 13). This clearly indicates the BA Tephra having more similar trace element concentrations to the HMA/HMBA series, as opposed to the low-Mg calc-alkaline series.

Implications

The data presented above suggests that the BA Tephra was sourced from the same magma family as the HMA/HMBA series, indicating a continuation of this magma source into the Holocene after eruption of the late Pleistocene lava flows. These eruptive units plot with a higher La/Yb ratio than the low-Mg calc-alkaline series. KKVF lavas from the HMA/HMBA series (higher La/Yb) that were erupted within the last 50 ka include the Glacier Creek andesite lava flow along Kulshan's south slope (~14 ka) and the Swift Creek basaltic andesite lava flow to the northeast (~48 ka) (Figure 14; Baggerman et al., 2011; Escobar et al., 2022). The Glacier Creek lava La/Yb ratio plots are like the average La/Yb ratio of the BA Tephra samples, with Glacier Creek lavas having La/Yb ~9-9.6 (Figure 14; Baggerman et al., 2011). Similarly, the Boulder Glacier assemblage and the Cathedral Crag lava (~331 ka), also sourced from the HMA/HMBA series, shows similar La/Yb ratios to the BA Tephra (La/Yb = ~9.5-11) (Baggerman et al. 2011; Moore et al., 2012). The Swift Creek lava flow plots on the lower end of La/Yb ratios (La/Yb = ~7-7.5) as does the Tarn Plateau lava flow (La/Yb ~7-8), but their magma

sourcing is still considered to be the HMA/HMBA series given their Mg# and other trace element characteristics (Figure 14; Escobar et al., 2022).

Figure 14 presents a timeline of La/Yb fluctuations over the last 800 ka years of magmatic eruptions from the KKVF. The basaltic andesite samples from the Sulphur Creek lava flow (~9.8 ka) plot on the higher La/Yb end of low-Mg calc-alkaline sourced eruptions than the basalts. On the other side, more SiO_2 rich samples from within the Dobbs Cleaver eruption (~105 ka), the Tarn Plateau eruption (~203 ka), and the Cougar Divide eruption (~613 ka) plot on the lower La/Yb end of HMA/HMBA sourced eruptions (Figure 14), suggesting some interaction of all of these magmas with an intermediate La/Yb silicic mixing endmember. All these eruptions straddle the boundary separating HMA/HMBA sourced and low-Mg source calc-alkaline eruptions. Further indicators of magma mixing, such as mingling and crystal clots, are needed to constrain the possibility of these two series mixing.

Based on the evidence and reasoning presented above, Figure 15 illustrates an updated conceptual model of the KKVF magma plumbing system within the last ~50 ka, where the low-Mg and HMA/HMBA systems are in close proximity. The dacitic remobilization involved the low-Mg Sulphur Creek basalt/basaltic andesite eruption is estimated to be at least ~20 km underneath the Schreiber Meadows edifice, with smaller mushes at greater depths (Garvey, 2020). Adjacent to the low-Mg magma system, the high-Mg basaltic andesite reservoir of the HMA/HMBA series is estimated to be at ~35 km depth, with liquid-depleted cumulates directly above the reservoir (Escobar, 2017; Valgardson, 2022). The results of this study suggest that there are two distinct but contemporaneous magma systems feeding the volcanic field in close proximity during the Holocene.

Given similarities in La/Yb of the silicic endmembers of the Sulphur Creek lava flow and the HMBA Swift Creek lava flow shown in Figure 14b (silicic endmembers plot nearest the low-Mg and high-Mg series La/Yb boundary), I've illustrated a possibility of these distinct magma series incorporating some component of laterally extensive dacitic mushes at depth.

Conclusions

This study considered the hypothesis that the sourcing of the BA Tephra was from the low-Mg calc-alkaline series that sourced the eruption of the (close-in-age) Sulphur Creek lava flow. Contrary to my original hypothesis, there are strong indications that the BA tephra was sourced from the HMA/HMBA series, as a continuation of the source of late Pleistocene lava flows. The major element contents of the BA Tephra glass are indicative of calc-alkaline magma sourcing (Figure 9). The BA Tephra has similar enrichments in Y, Zr, Ba, La, and Yb, and similar depletions in Sr to the HMA/HMBA series (Figure 10). Both the BA Tephra and the HMA/HMBA series are characterized by a higher La/Yb ratio, ranging from 7-12 (Figure 12). Previous studies of the BA Tephra included bulk composition XRF analyses. However, this study presents the first comprehensive geochemical analyses done on the BA Tephra glass.

Future work on the BA Tephra should include characterizing mineral populations. This includes obtaining major and trace element concentrations in zoned phenocrysts to understand the depth of crystallization. Additionally, future work on the KKVF magma system should include constraining indicators of magma mixing between dacite mushes hypothesized to lie beneath the HMA/HMBA series and low-Mg calc-alkaline series.

References

Bacon, C.R., 1983, Eruptive history of Mount Mazama and Crater Lake caldera, Cascade Range, U.S.A.: Journal of Volcanology and Geothermal Research, v. 18, p. 57–115.

Baggerman, T.D., and DeBari, S.M., 2011, The generation of a diverse suite of Late Pleistocene and Holocene basalt through dacite lavas from the northern Cascade arc at Mount Baker, Washington: Contributions to Mineralogy and Petrology, v. 161, p. 75–99.

Brown, E.H., 1987, Structural geology and accretionary history of the Northwest Cascades system, Washington, and British Columbia: Geological Society of America Bulletin, 99, 201-214.

Escobar, R., 2016, Mineral Complexities as Evidence for Open-system Processes in Formation of Intermediate Magmas of the Mount Baker Volcanic Field, Northern Cascade Arc: WWU Graduate School Collection, doi: https://doi.org/10.25710/99fs-s849.

Escobar, R., DeBari, S.M., 2021 (in progress), Long-lived, variable-composition crystal mushes beneath a Cascade volcano, evidence from crystal clots and phenocrysts in Koma Kulshan (Mt. Baker) lavas, northern Cascade Arc: AGU Fall Meeting 2021, held in New Orleans, LA, 13-17 December 2021, id. V11A-04.

Garvey, B., 2022, Using crystal zoning, thermobarometry, and MELTS to elucidate Koma Kulshan's (Mt. Baker) transcrustal magma storage system, northern Cascade arc: WWU Graduate School Collection, 1122, https://cedar.wwu.edu/wwuet/1122.

Green, N.L., and Harry, D.L. (1999) On the relationship between subducted slab age and arc basalt petrogenesis, Cascadia subduction system, North America: Earth and Planetary Science Letters, 171, 367-381.

Griffin, W.L., Powell, W.J., Pearson, N.J., O`Reilly, S.Y., 2008, GLITTER: data reduction software for laser ablation ICP-MS: Minerological Association of Canada Short Course 40, Vancouver, B.C., p. 308-311.

Gross, J.A., 2012, Felsic magmas from Mt. Baker in the northern Cascade arc: origin and role in andesite production: WWU Graduate School Collection, 239, doi: https://doi.org/10.25710/3j48-ah29.

Grove, T. L., Baker, M. B., Price, R. C., Parman, S. W., Elkins-Tanton, L. T., Chatterjee, N., & Müntener, O. (2005). Magnesian andesite and dacite lavas from Mt. Shasta, northern California: products of fractional crystallization of H 2 O-rich mantle melts. Contributions to Mineralogy and Petrology, 148, 542-565.

Hildreth, W., Fierstein, J., and Lanphere, M., 2003, Eruptive history and geochronology of the Mount Baker volcanic field, Washington: Geological Society of American Bulletin, p. 729-764.

Jochum, K.P., Willbold, M., Raczek, I., Stoll, B., Herwig, K., 2005, Chemical Characterisation of the USGS Reference Glasses GSA-1G, GSC-1G, GSD-1G, GSE-1G, BCR-2G, BHVO-2G and BIR-1G Using EPMA, ID-TIMS, ID-ICP-MS and LA-ICP-MS: Geostandards and Geoanalytical Research, v. 29, p. 285-302.

McCrory PA, Blair JL, Oppenheimer DH, Walter SR (2004) Depth to the Juan de Fuca slab beneath the Cascadia subduction margin— a 3-D model for sorting earthquakes. U.S. Geological Survey Data Series 91, CD-Rom Version 1.2, July 13, 2009, p 13.

Misch, P., 1966, Tectonic evolution of the Northern Cas- cades of Washington State; A West Cordilleran case history, in Gunning, H.C., ed., A symposium on the tectonic history and mineral deposits of the western Cordillera: Canadian Institute of Mining and Metal- lurgy Sepcial Volume 8, p. 101–148.

Moore, N.E., DeBari, S.M., 2012, Mafic magmas from Mount Baker in the northern Cascade arc, Washington: probes into mantle and crustal processes: Contributions to Mineralogy and Petrology, v. 163, p. 521–546.

Scott, K.M., Tucker, D.S., Riedel, J.L., Gardner, C.A., and McGeehin, J.P., 2020, Latest Pleistocene to Present Geology of Mount Baker Volcano, Northern Cascade Range, Washington: Professional Paper U.S. Geological Survey Professional Paper 1865.

Sas, M., DeBari, S.M., Clynne, M.A., and Rusk, B.G., 2017, Using mineral geochemistry to decipher slab, mantle, and crustal input in the generation of high-Mg andesites and basaltic andesites from the northern Cascade Arc: American Mineralogist, v. 102, p. 948–965.

Tabor, R.W., Haugerud, R.A., Hildreth, W., and Brown, E.H., 2003, Geologic map of the Mount Baker 30 x 60-minute quadrangle, Washington: U.S. Geological Survey Map I-2660, scale 1:100,000, 2 sheets.

Valgardson, H., 2022 (unpublished), Indicators for the magmatic architecture beneath Koma-Kulshan (Mt. Baker) by using crystals in lava flows: WWU Undergraduate Collection.

Tables

Element	avg	2sd	reported	precision %	accuracy
Na23	28354	438	28339	2	0.05
Mg25	21598	202	21595	1	0.01
Al27	72500	0		0	
Si29	245548	3506	245438	1	0.04
K39	25081	311	25071	1	0.04
Ca43	51528	1138	51530	2	0.00
Sc45	53.00	0.76	53.00	1	0.00
Ti47	7796	114	7794	1	0.03
Ti49			7794		
V51			47.00		
Fe57	103415	1286	103381	1	0.03
Ni60	56.52	1.97	56.50	3	0.04
Rb85	38.03	1.07	38.00	3	0.08
Sr88	69.50	1.58	69.50	2	0.00
Y89	45.00	0.80	45.00	2	0.01
Zr90	44.62	1.13	44.60	3	0.04
Nb93	46.03	1.17	46.00	3	0.07
Cs133	32.32	0.92	32.30	3	0.07
Ba137	69.42	2.34	69.40	3	0.03
La139	40.01	1.06	40.00	3	0.03
Ce140	41.21	1.14	41.20	3	0.02
Pr141	46.11	1.26	47.67	3	3.28
Nd146	44.88	1.65	44.90	4	0.04
Sm147	47.64	1.80	47.60	4	0.08
Eu153	40.81	1.26	40.80	3	0.03
Gd157	50.24	2.27	50.20	5	0.08
Tb159	49.63	1.71	49.60	3	0.06
Dy163	53.23	2.28	53.20	4	0.06
Ho165	51.13	1.88	51.10	4	0.05
Er166	39.62	1.38	39.60	3	0.06
Tm169	51.91	1.67	51.90	3	0.02
Yb171	53.42	2.41	53.40	5	0.04
Lu175	54.72	1.69	54.70	3	0.03
Hf178	40.93	1.79	40.90	4	0.07
Ta181	44.43	1.71	44.40	4	0.06
Pb206	51.24	1.90	51.20	4	0.08
Pb207	51.24	2.27	51.20	4	0.07
Pb208	51.23	1.87	51.20	4	0.05
Th232	43.64	2.48	43.60	6	0.10
U238	40.63	1.85	40.60	5	0.09

Table 1. LA-ICP-MS standard analyses (ppm) of USGS glass standard GSD-1G (n=15). Al27 is marked in red to denote as an internal standard for analysis.

Element	avg	2sd	reported	precision %	accuracy
Na23	30544	457	30416	1	0
Mg25	21376	202	21052	1	2
Al27	70913	0		0	
Si29	244922	2947	247008	1	1
K39	21700	355	22082	2	2
Ca43	52731	778	51959	1	1
Sc45	540.66	5.69	540.00	1	0
Ti47	447	9	480.00	2	7
Ti49			480.00		
V51			460.00		
Fe57	100955	1379	98717	1	2
Ni60	426.15	7.92	431.00	2	1
Rb85	371.21	5.77	361.00	2	3
Sr88	454.06	6.32	444.00	1	2
Y89	457.09	5.21	449.00	1	2
Zr90	436.03	6.48	427.60	1	2
Nb93	469.92	7.44	456.00	2	3
Cs133	314.56	6.33	301.00	2	5
Ba137	438.06	9.38	419.00	2	5
La139	407.82	8.56	392.00	2	4
Ce140	420.91	9.52	405.00	2	4
Pr141	480.55	10.96	460.00	2	4
Nd146	464.72	12.72	449.00	3	4
Sm147	494.29	12.79	478.00	3	3
Eu153	417.81	8.99	403.00	2	4
Gd157	529.10	11.75	514.00	2	3
Tb159	519.91	12.69	501.00	2	4
Dy163	549.81	10.61	535.00	2	3
Ho165	532.60	12.73	511.00	2	4
Er166	614.94	14.96	598.00	2	3
Tm169	539.76	9.30	519.00	2	4
Yb171	554.11	13.21	540.00	2	3
Lu175	562.64	15.42	536.00	3	5
Hf178	419.97	9.63	406.00	2	3
Ta181	453.59	11.55	426.00	3	6
Pb206	407.87	12.88	366.20	3	11
Pb207	405.14	15.26	366.20	4	11
Pb208	405.93	13.50	366.20	3	11
Th232	414.82	26.07	391.60	6	6
U238	417.89	11.08	377.60	3	11

Table 2. LA-ICP-MS standard analyses (ppm) of USGS glass standard GSE-1G (n=15). Al27 is marked in red to denote as an internal standard for analysis.

Element	avg	2sd	reported	precision %	accuracy
Na23	17704	315	17805	2	1
Mg25	45011	654	43008	1	5
Al27	71971	0		0	
Si29	23488 1	4775	230478	2	2
K39	4279	75	4234	2	1
Ca43	82206	1415	81476	2	1
Sc45	32.96	0.70	NA	2	
Ti47	16551	229	16666	1	1
Ti49			16666		
V51			NA		
Fe57	92459	3724	87835	4	5
Ni60	121.27	2.37	112.00	2	8
Rb85	9.45	0.30	8.89	3	6
Sr88	393.36	6.10	389.00	2	1
Y89	26.45	0.65	27.20	2	3
Zr90	174.13	2.73	175.00	2	0
Nb93	18.66	0.42	18.10	2	3
Cs133	0.10	0.02	0.09	21	12
Ba137	132.26	3.52	127.00	3	4
La139	15.43	0.47	15.80	3	2
Ce140	37.26	0.66	36.00	2	3
Pr141	5.22	0.15	5.16	3	1
Nd146	24.33	1.40	24.30	6	0
Sm147	6.12	0.43	6.07	7	1
Eu153	2.05	0.16	2.10	8	2
Gd157	6.29	0.51	6.35	8	1
Tb159	0.93	0.07	0.96	7	3
Dy163	5.34	0.36	5.47	7	2
Ho165	0.97	0.09	1.03	9	5
Er166	2.54	0.18	2.56	7	1
Tm169	0.33	0.04	0.34	11	4
Yb171	2.04	0.21	2.13	10	4
Lu175	0.29	0.04	0.29	13	0
Hf178	4.50	0.33	4.60	7	2
Ta181	1.14	0.07	1.15	6	1
Pb206	1.89	0.23	1.75	12	8
Pb207	1.99	0.35	1.75	17	14
Pb208	1.97	0.17	1.75	8	13
Th232	1.29	0.09	1.27	7	2
U238	0.43	0.05	0.41	11	4

Table 3. LA-ICP-MS standard analyses (ppm) of USGS glass standard BHVO-2G (n=15). Al27 is marked in red to denote as an internal standard for analysis.

Figures

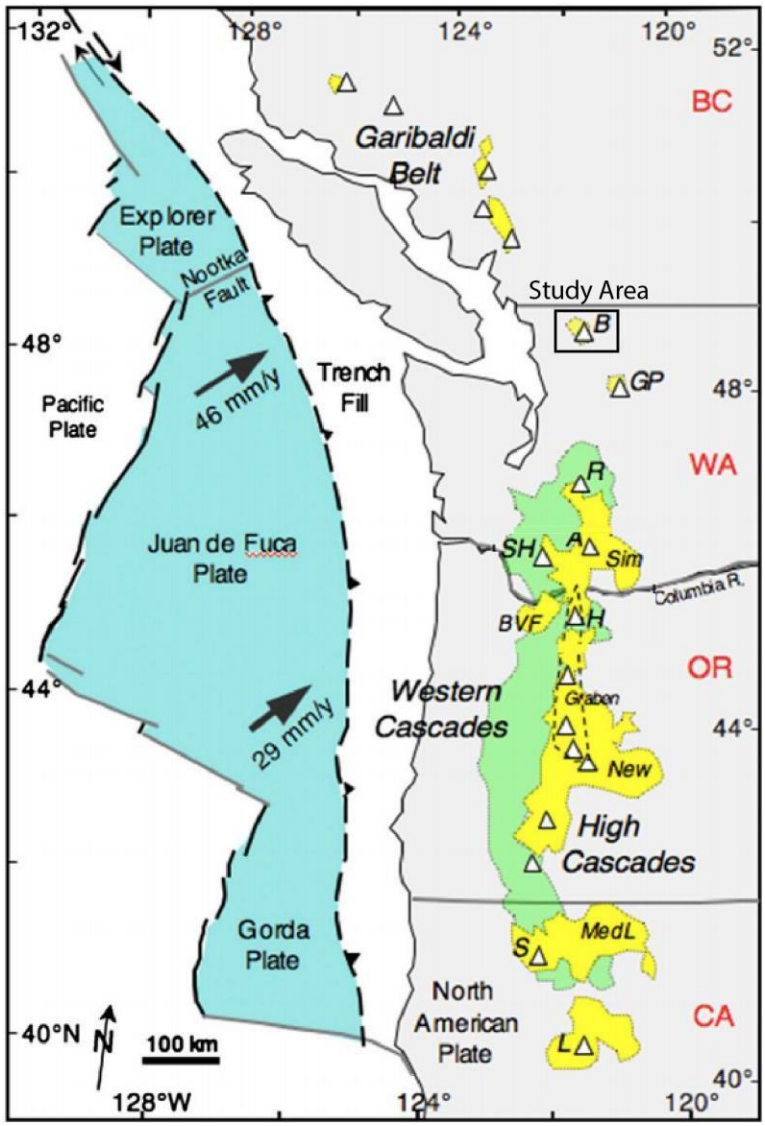

Figure 1. Map of the Cascade Volcanic Arc from southern British Columbia to northern California. Each triangle denotes major stratovolcanoes along the Cascade Range with label as follows: B = Mount Baker (Koma Kulshan), GP = Glacier Peak, R = Mount Rainier, A = Mount Adams, SH = Mount Saint Helens, H = Mount Hood, S = Mount Shasta, and L = Lassen Peak. Koma Kulshan is marked as study area, modified by Garvey, 2022, and modified from Leeman, 2020.

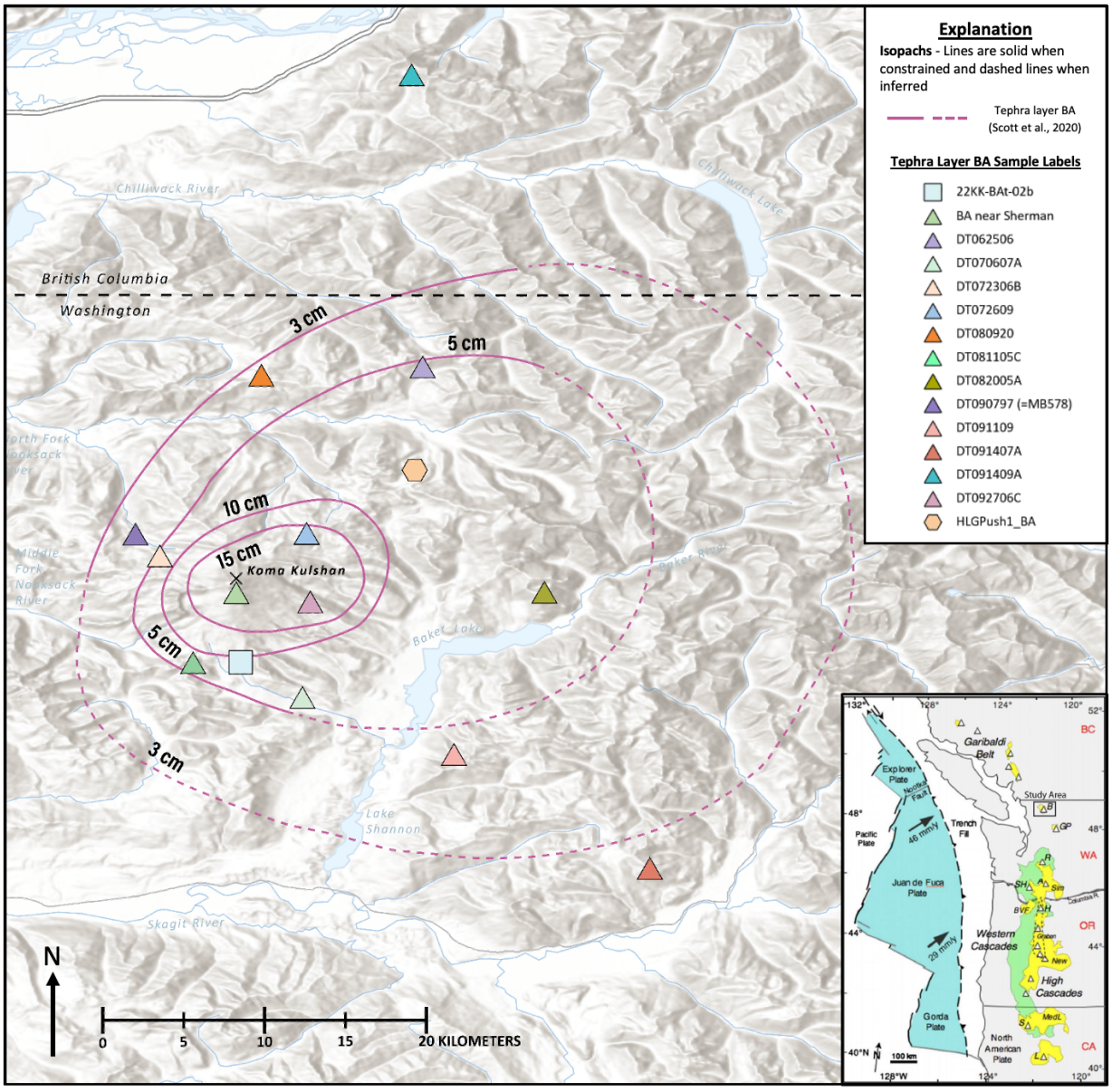

Figure 2. Map of Tephra Layer BA distribution with isopachs of 15, 10, 5, and 3 cm deposit thickness. Samples utilized in the study are plotted with UTM data points of site collection. Inset map is from Figure 1.

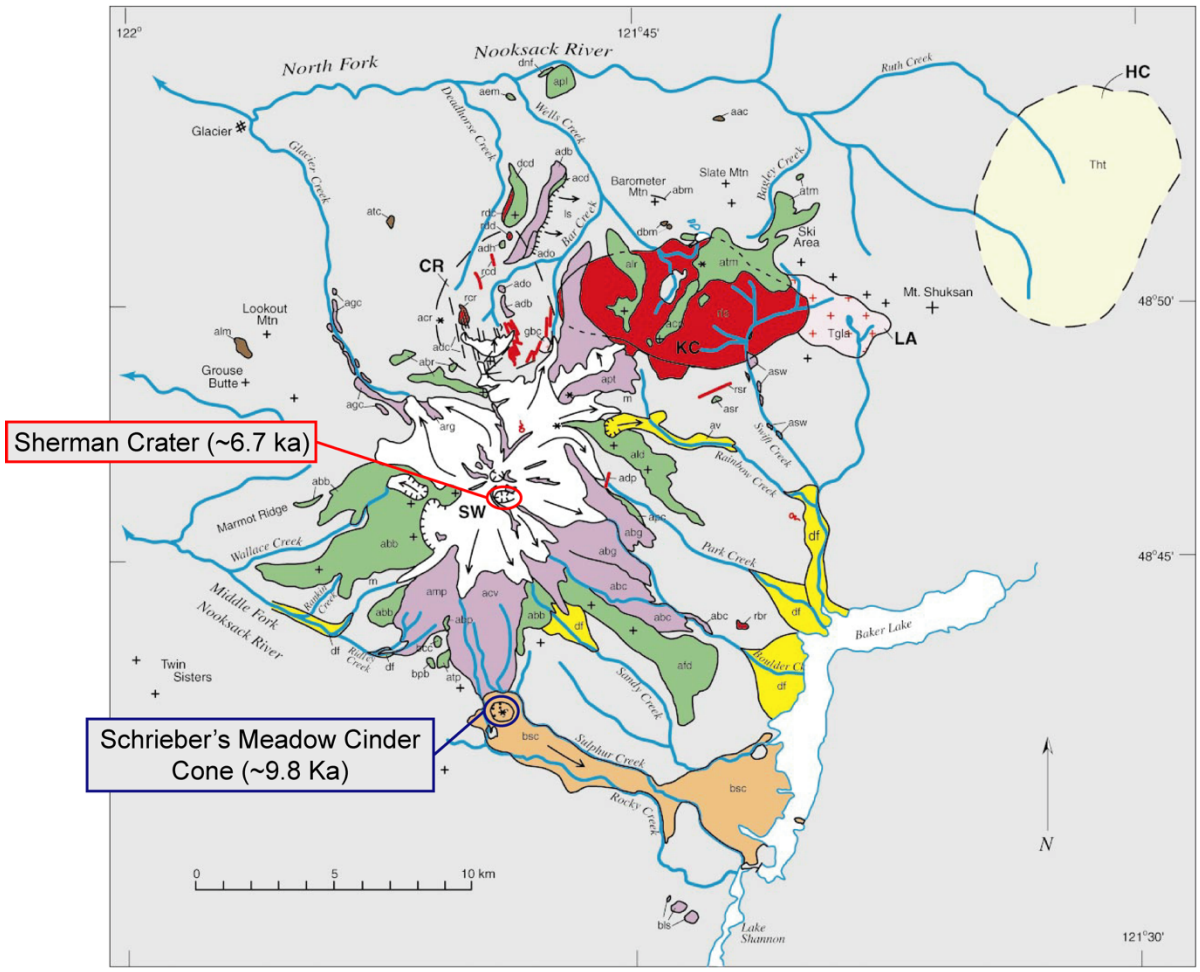

Figure 3. Geologic map of eruptive units from the KKVF by Hildreth et al., 2003. Sherman Crater and Schreiber's Meadow Cinder Cone are highlight. Glaciers on the Koma Kulshan edifice are colored in white. Holocene eruptive units, such as the Sulphur Creek basalt, are colored in orange. Late Pleistocene lava flows are colored in purple. Middle Pleistocene lava flows are colored in green. Early Pleistocene Kulshan caldera is colored in red. Debris flows are colored in yellow.

Figure 4. Image organization process for each glass spot, with decreasing scale from top to bottom. The yellow rectangle is a confined parallelogram used to collect constrained spectra on the SEM, with a diameter of ~30-50 µm. Sample DT091109 is imaged in this figure.

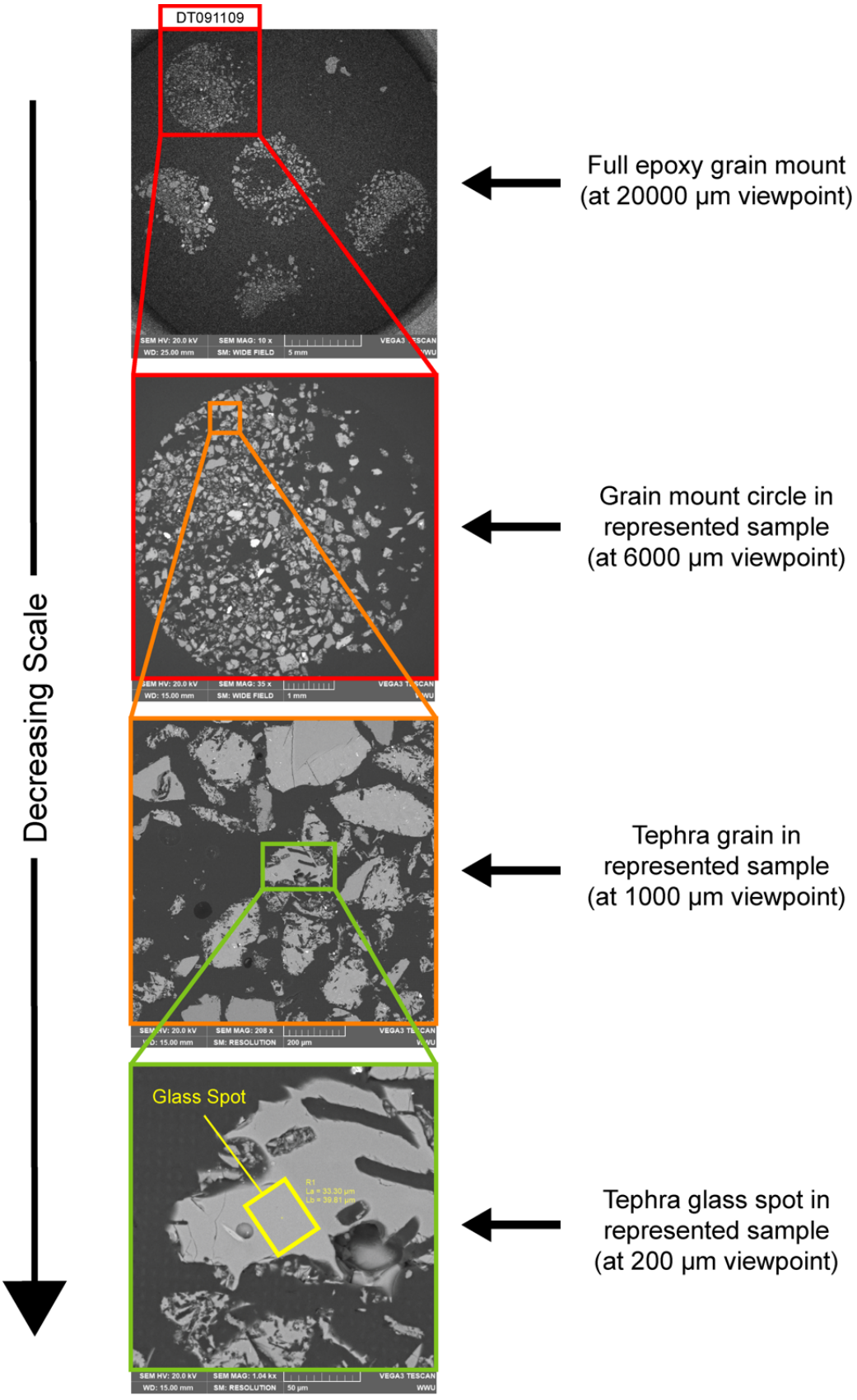

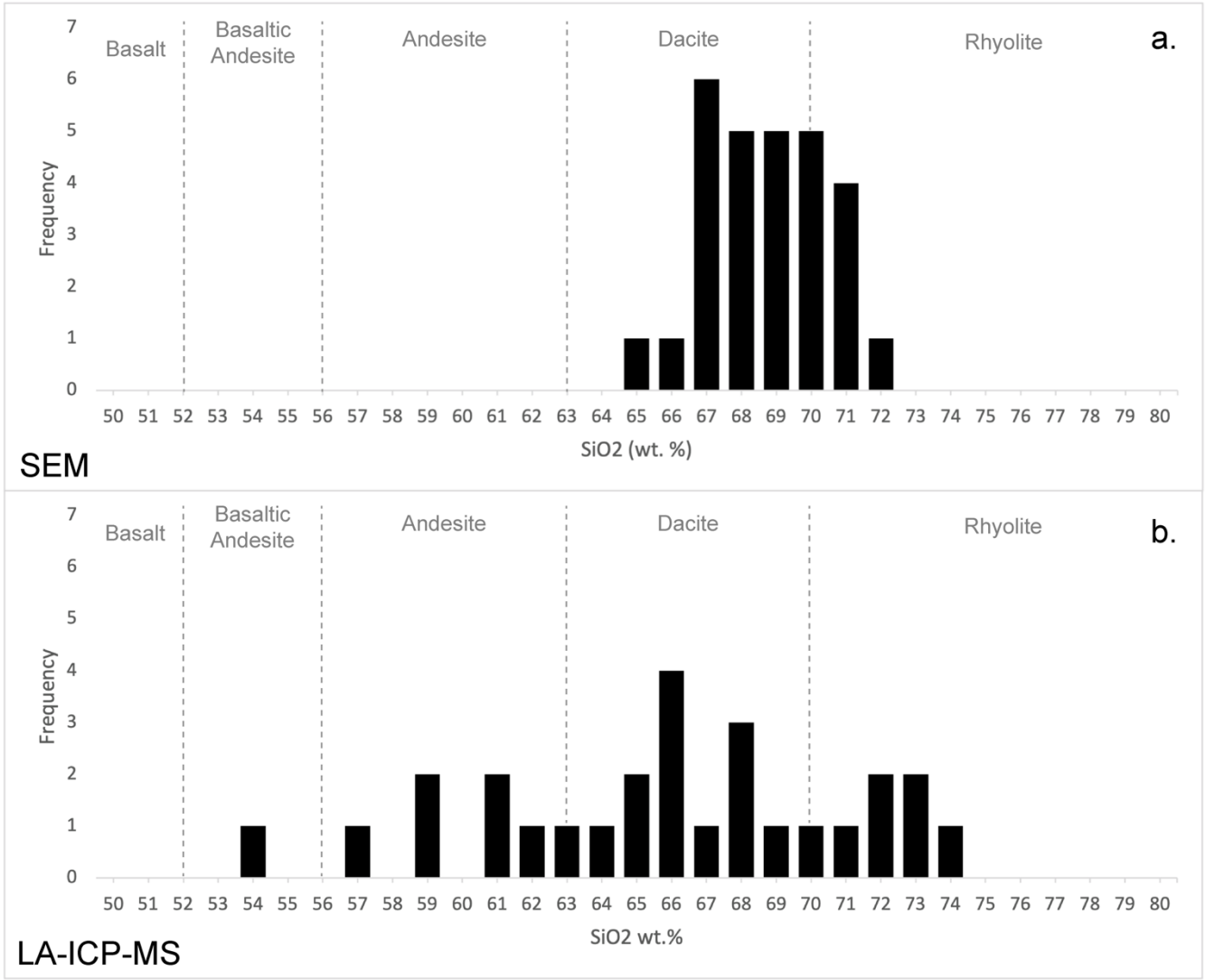

Figure 5. Histograms of distribution of SiO_2, where a) is from analyses using the SEM and b) is from analyses using the LA-ICP-MS, with fields marking magma compositions accordingly.

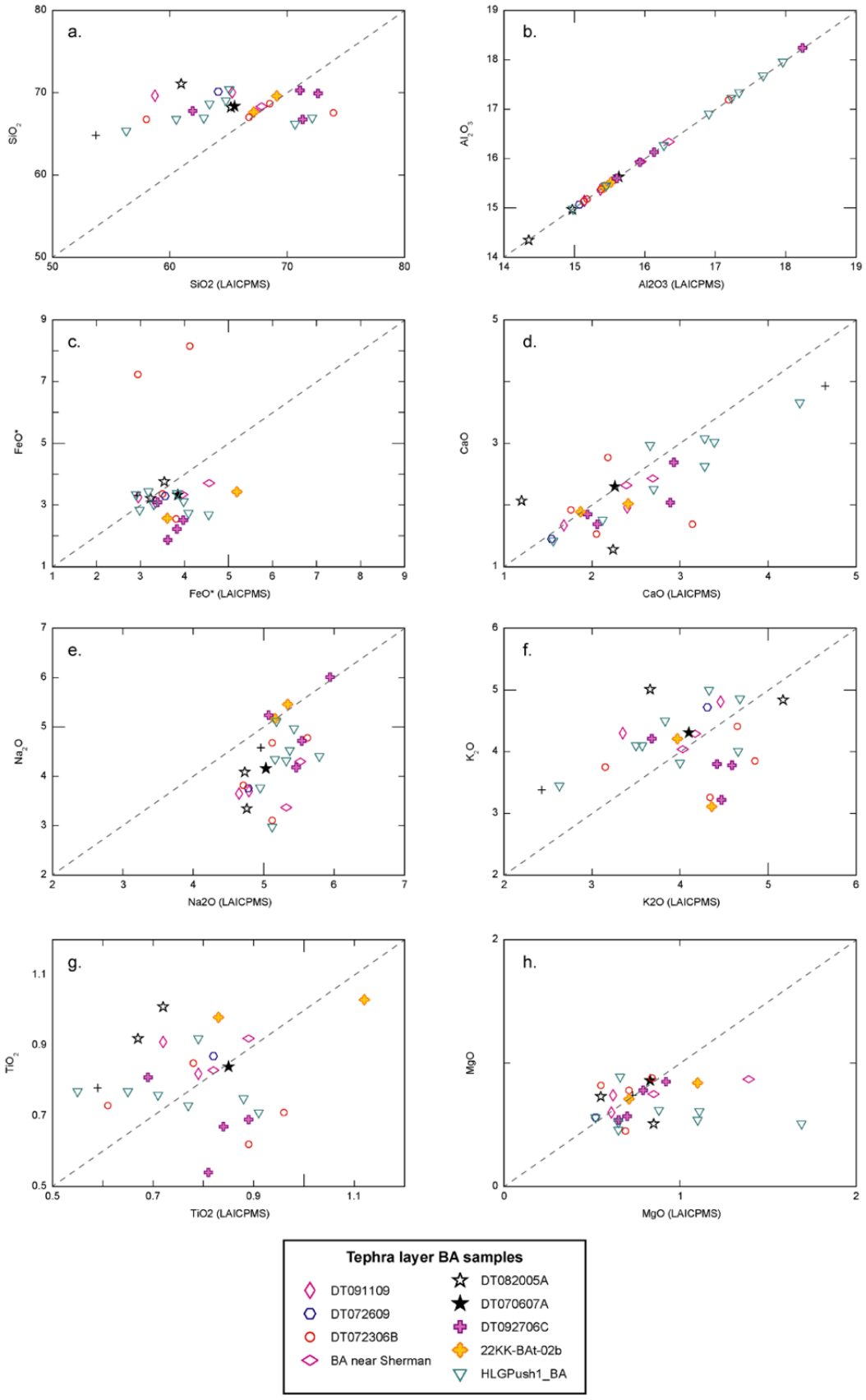

Figure 6. Comparative major element oxide data for analyses obtained by SEM (plotted on y-axis for each oxide, a-h) and for analyses obtained by LA-ICP-MS (plotted on x-axis for each oxide, a-h). The dashed line represents one-to-one correlation of oxide concentrations between methods.

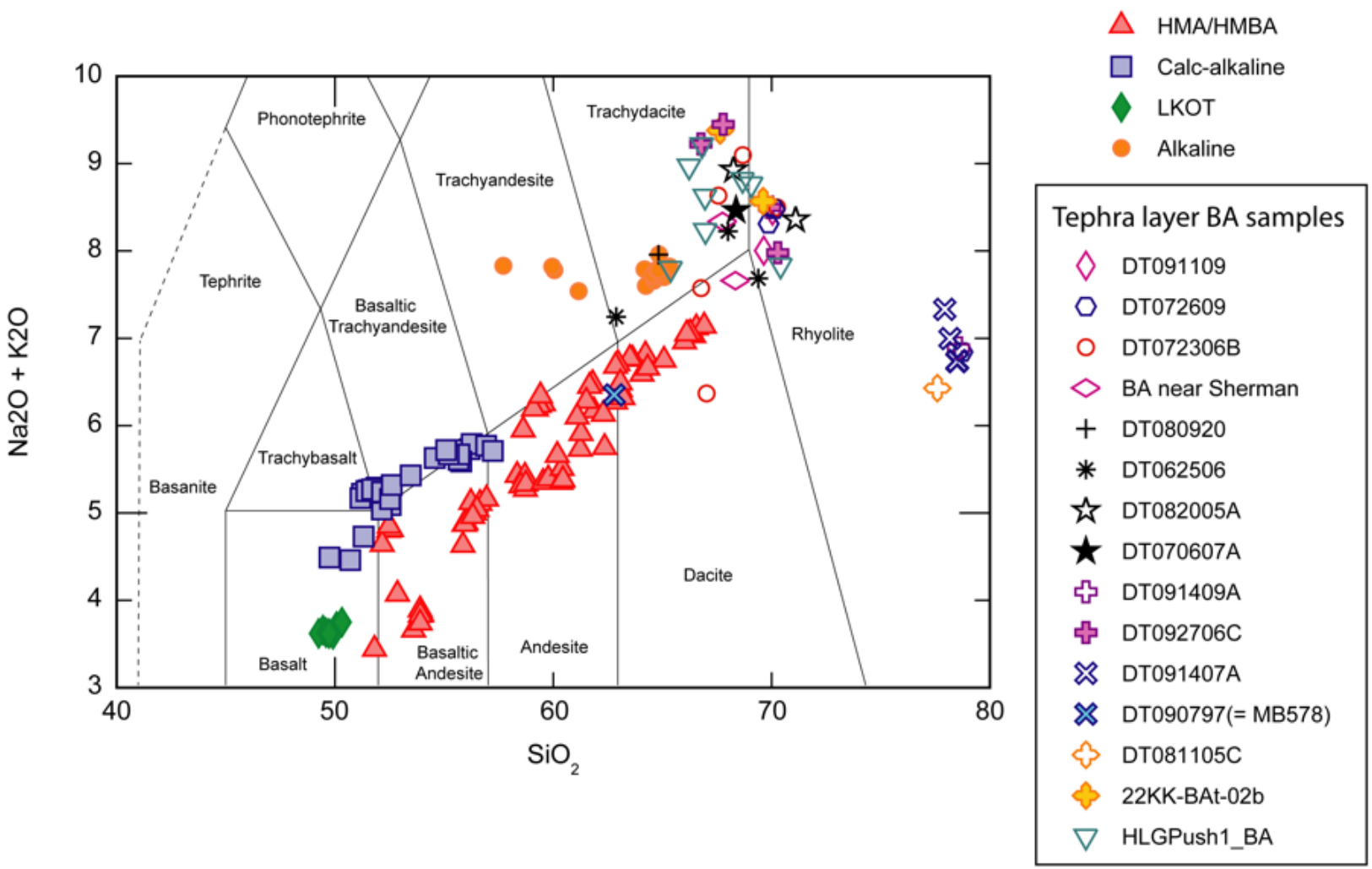

Figure 7. Total Alkali-Silica Plot of BA tephra glass analyses (multiple symbols) (see Appendix 1 for data) and whole rock data from lavas in the HMA/HMBA series (red triangles) (from Baggerman, 2011, Gross, 2012, Moore, 2012, and Escobar, 2022), the low-Mg calc-alkaline series (blue squares) (from Moore, 2012 and Garvey, 2022), the LKOT series (green diamonds) (from Moore, 2012), and the Alkaline series (orange circles) (from Gross, 2012 and Escobar, 2022). See text for discussion of high-Si glass analyses that are not part of the BA tephra.

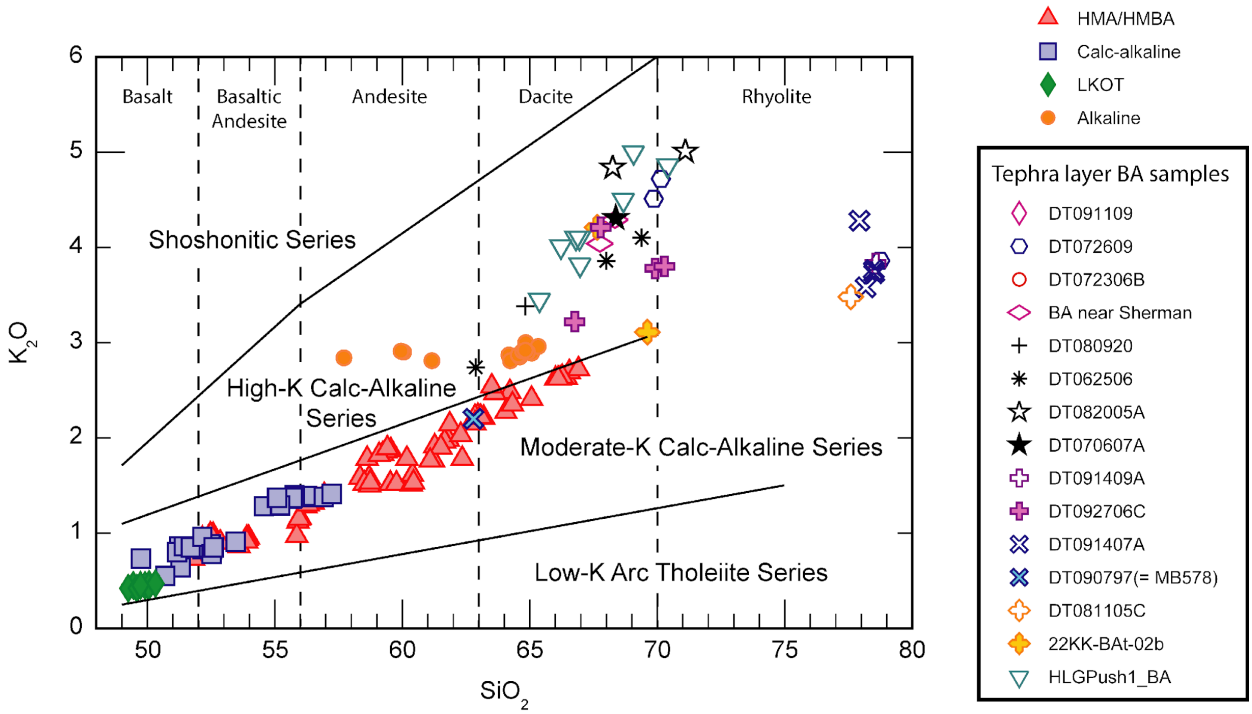

Figure 8. K_2O vs. SiO_2 plot of BA tephra glass analyses and whole rock data from lavas in the HMA/HMBA series (red triangles), the low-Mg calc-alkaline series (blue squares), the LKOT series (green diamonds), and the Alkaline series (orange circles). Data sources as in Figure 7. See text for discussion of high-Si glass analyses that are not part of the BA tephra.

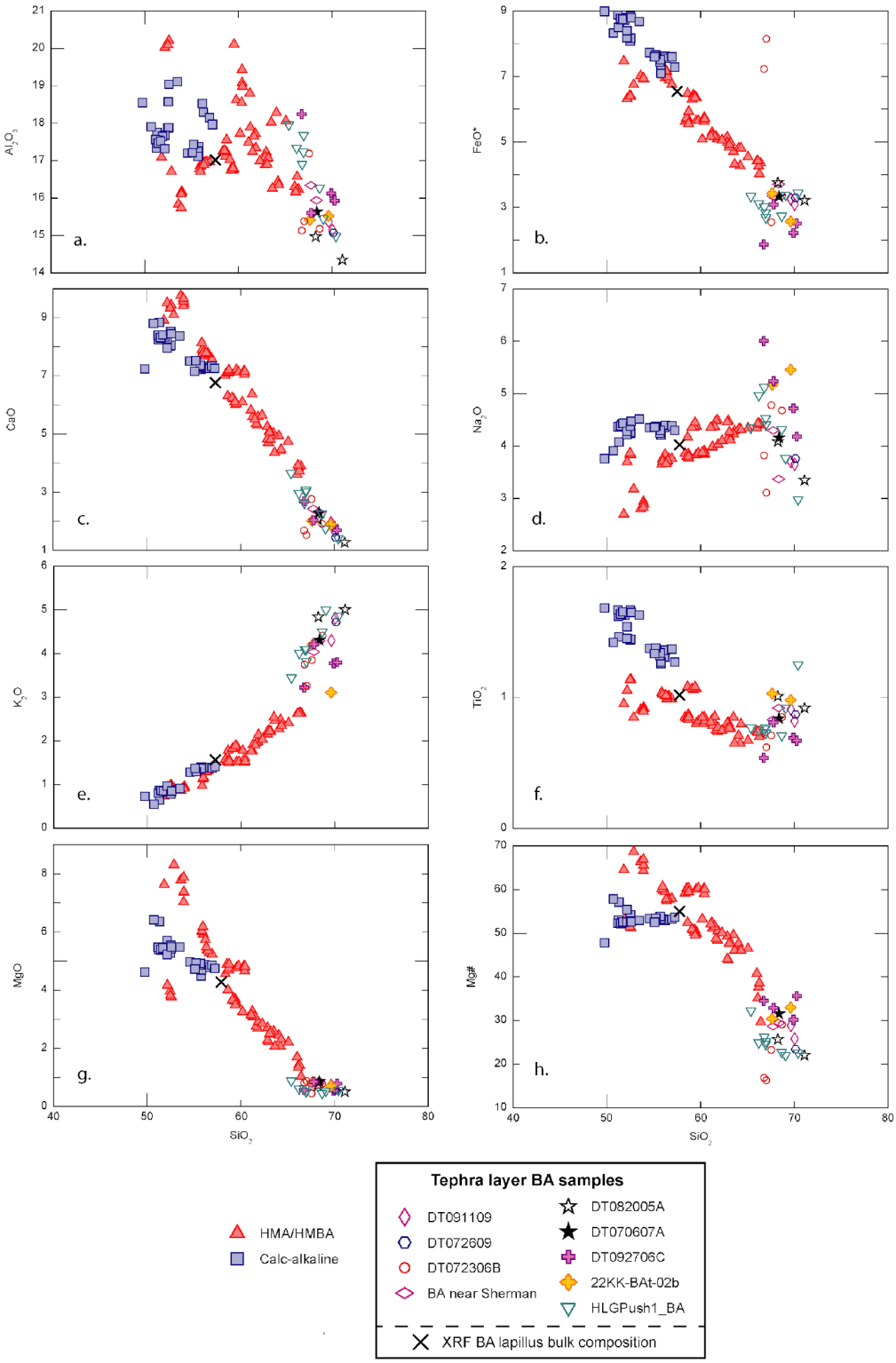

Figure 9. Harker diagrams of major element oxide percents from BA tephra glass spots plotted on the y-axis against wt.% SiO_2 plotted on the x-axis, including a) Al_2O_3, b) FeO, c) CaO, d) Na_2O, e) K_2O, f) TiO_2, g) MgO, and h) Mg# (100*Mg/(Mg+Fe). See Appendix 1 for data. BA tephra bulk lapillus by XRF from Hildreth et al., 2003. Bulk rock compositions of lavas from the HMA/HMBA series and the low-Mg calc-alkaline series samples are also displayed. References as in Figure 7.

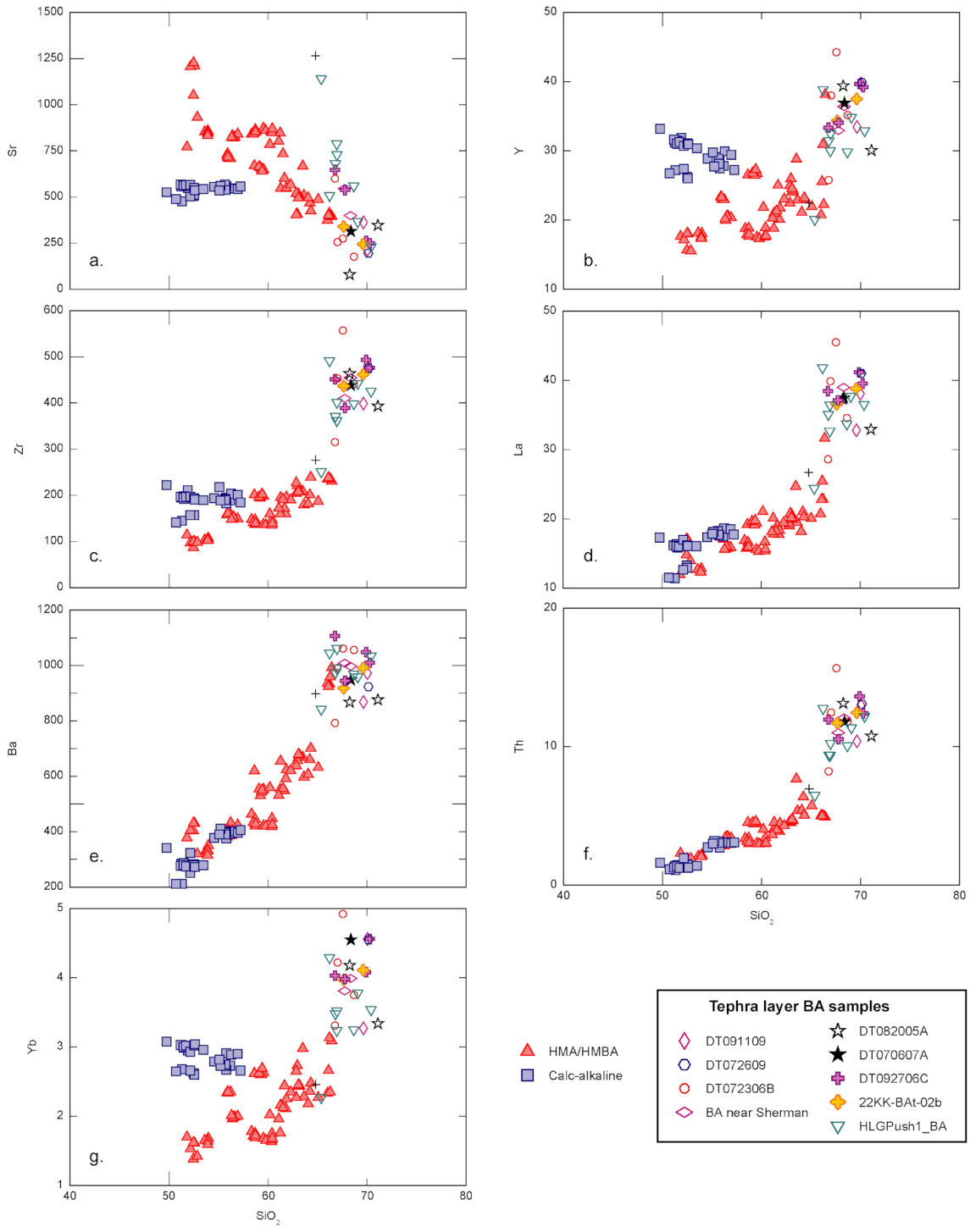

Figure 10. Harker diagrams of select trace elements concentrations from BA tephra glass spots (in ppm) plotted on the y-axis against wt.% SiO_2 plotted on the x-axis, including a) Sr, b) Y, c) Zr, d) La, e) Ba, f) Th, and g) Yb. See Appendix 2 for data. Bulk rock compositions of lavas from the HMA/HMBA series and the low-Mg calc-alkaline series samples are also displayed.

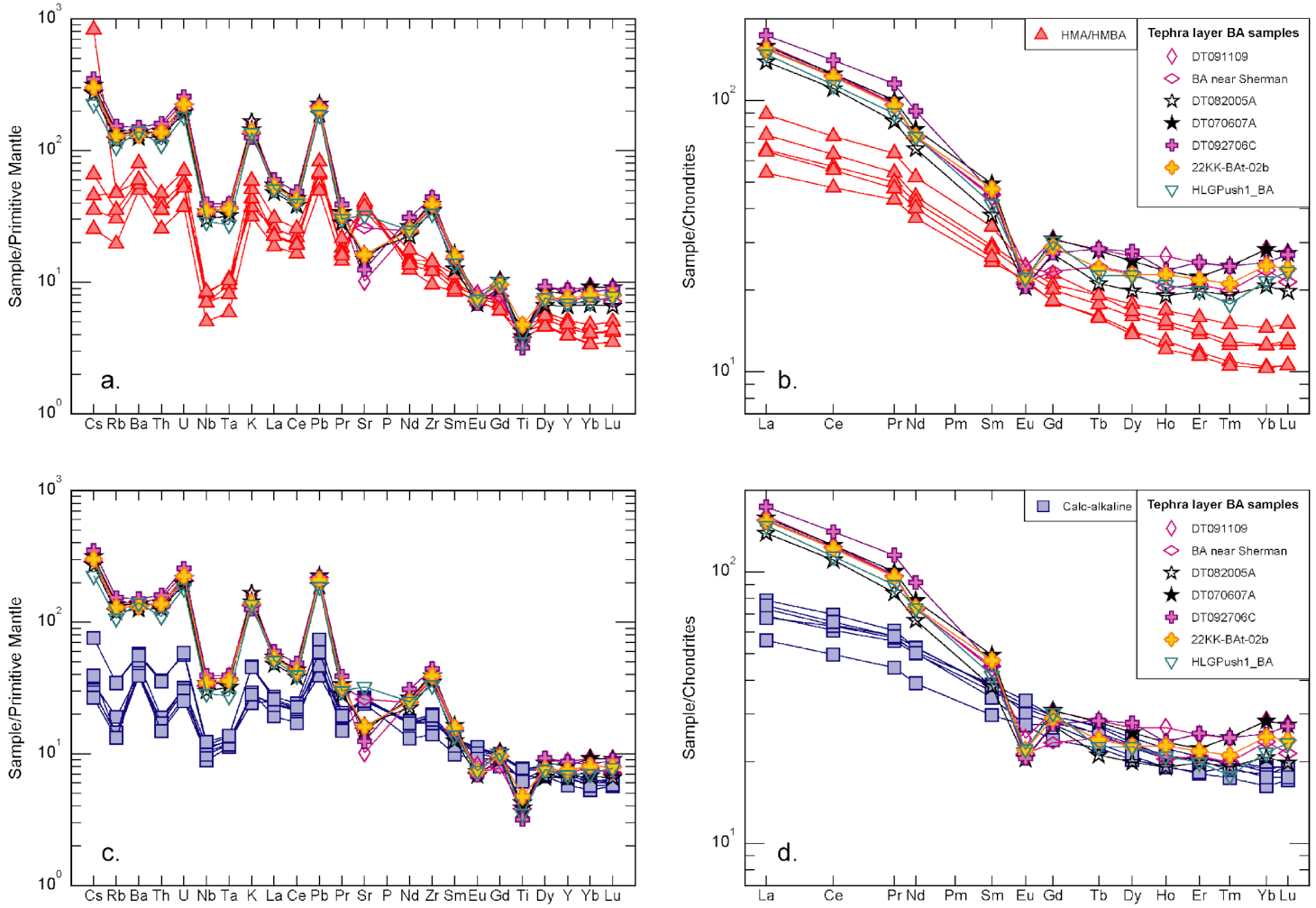

Figure 11. a) & c) Extended trace element diagrams normalized to primitive mantle and b) & d) REE diagrams normalized to chondrite. Representative BA tephra glass analyses and HMA/HMBA series (a & b) and low-Mg calc-alkaline series (c & d) whole rock lavas are also plotted. Samples used in a) are the same in b), and samples used in c) are the same in d). HMA/HMBA series samples are as follows: Tarn Plateau basaltic andesite (~203 ka; NM-TP2) from Moore et al. (2012), Swift Creek andesite (~48 ka; asw-33) and Dobbs Creek andesite (~119 ka; ado-14) from Escobar et al. (2022), and Glacier Creek andesite (~14 ka; GC-2TB) and Boulder Glacier andesite (~90 ka; BG-4TB) from Baggerman et al. (2011). Low-Mg calc-alkaline series samples are as follows: Lake Shannon basaltic andesite (~94 ka; NM-LS2) and Sulphur Creek basalt (~9.8 ka; NM-SC3) from Moore et al. (2012), Sulphur Creek basalts (2012-SC-Tephra-2, 2020-SC1, & 2020-SC2) from Garvey et al. (2022), and Sulphur Creek basaltic andesites (QBSC-3 & SC-1TB) from Baggerman et al. (2011).

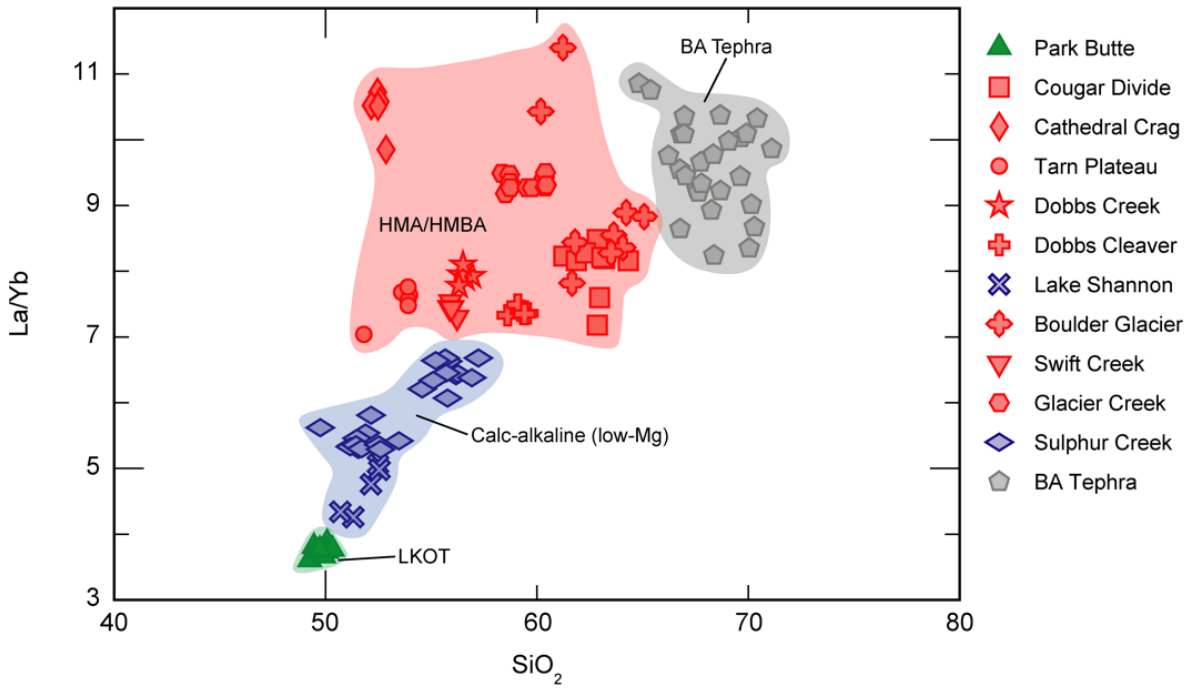

Figure 12. La/Yb ratio vs. SiO_2 with glass analyses from the BA tephra (grey), whole rock lava data from the HMA/HMBA series (red), low-Mg calc-alkaline series (blue), and the LKOT series (green).

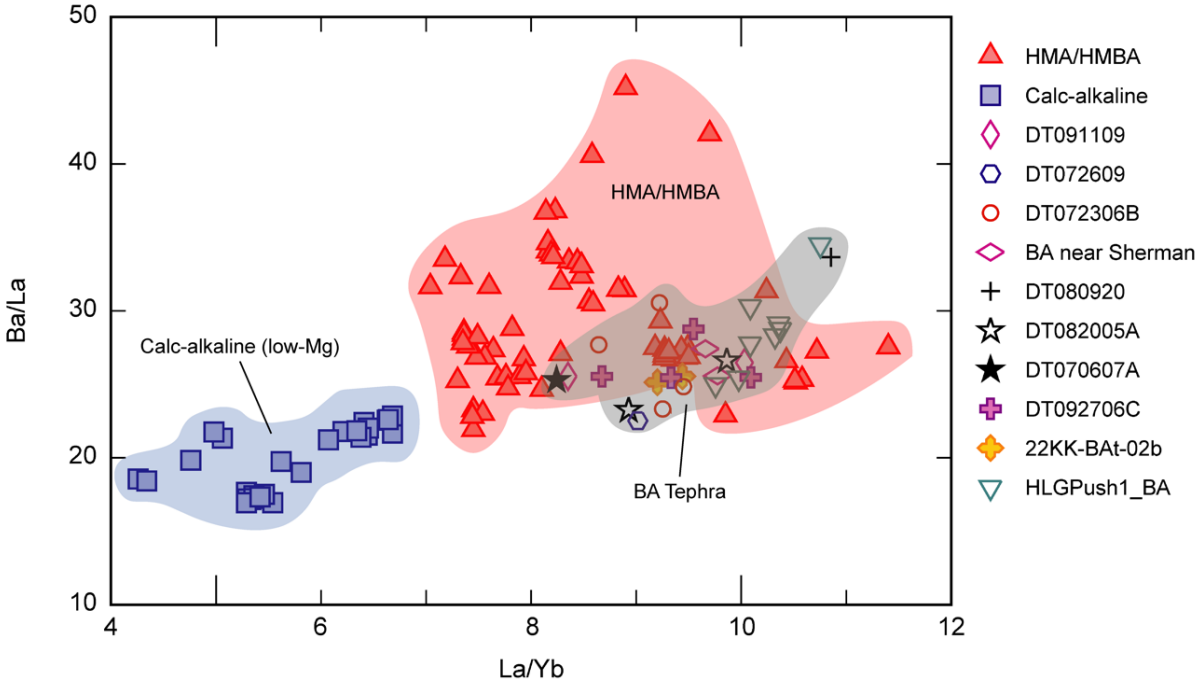

Figure 13. Ba/La vs. La/Yb, with glass analyses from the BA tephra (grey), and whole rock lava data from the HMA/HMBA series (red) and low-Mg calc-alkaline (blue).

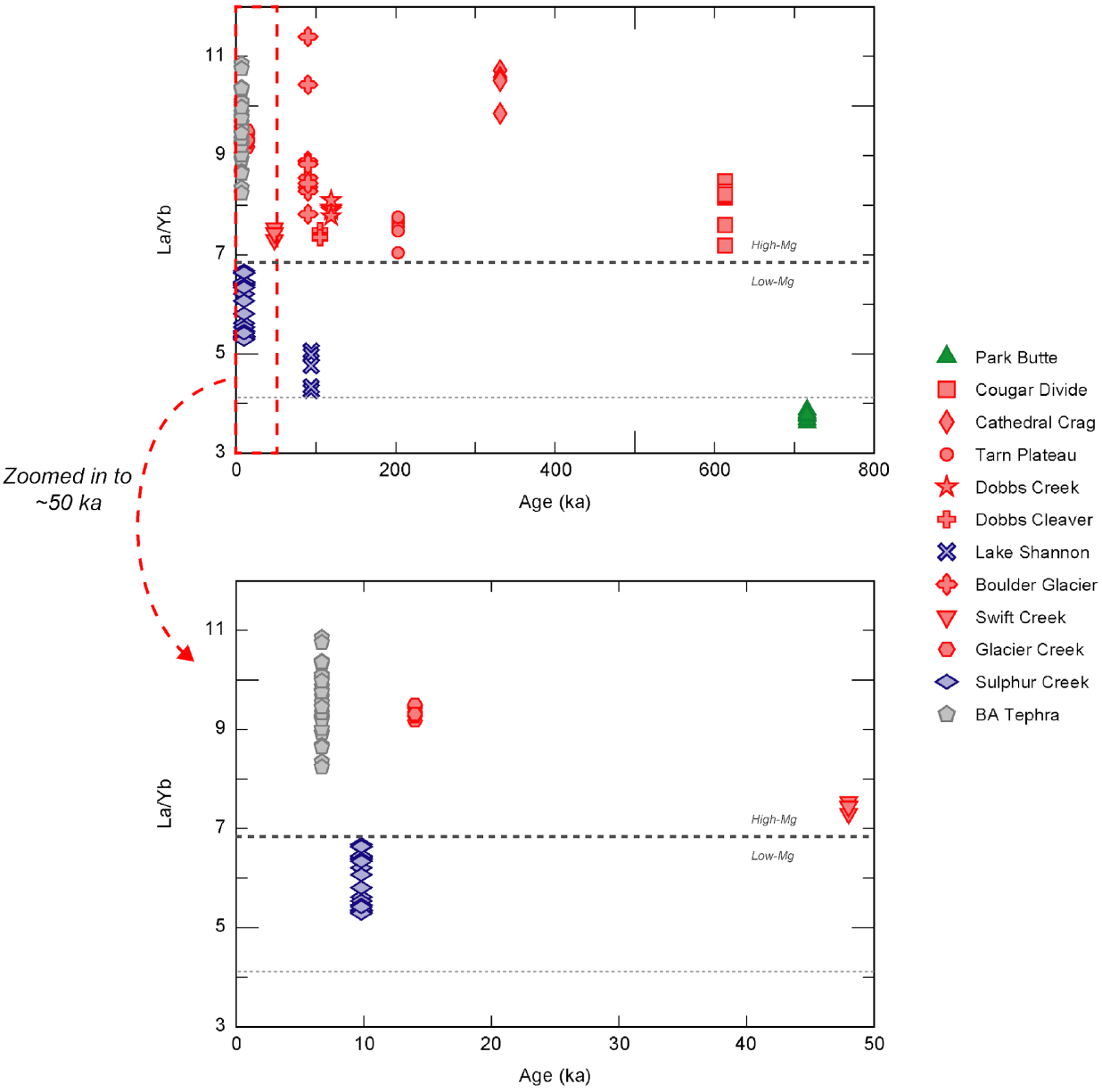

Figure 14. La/Yb ratio vs. age of eruption for BA tephra samples (grey), the HMA/HMBA series (red), the low-Mg calc-alkaline series (blue), and the LKOT series (green). The dark grey dashed line represents the threshold between high-Mg magmas and low-Mg magmas, based on La/Yb. The light grey dashed line indicates the difference between plotted eruptions sourced from the low-Mg calc-alkaline and the LKOT series. The bottom plot is zoomed in within the last 50 ka, as noted by the dashed red lined box on the upper plot.

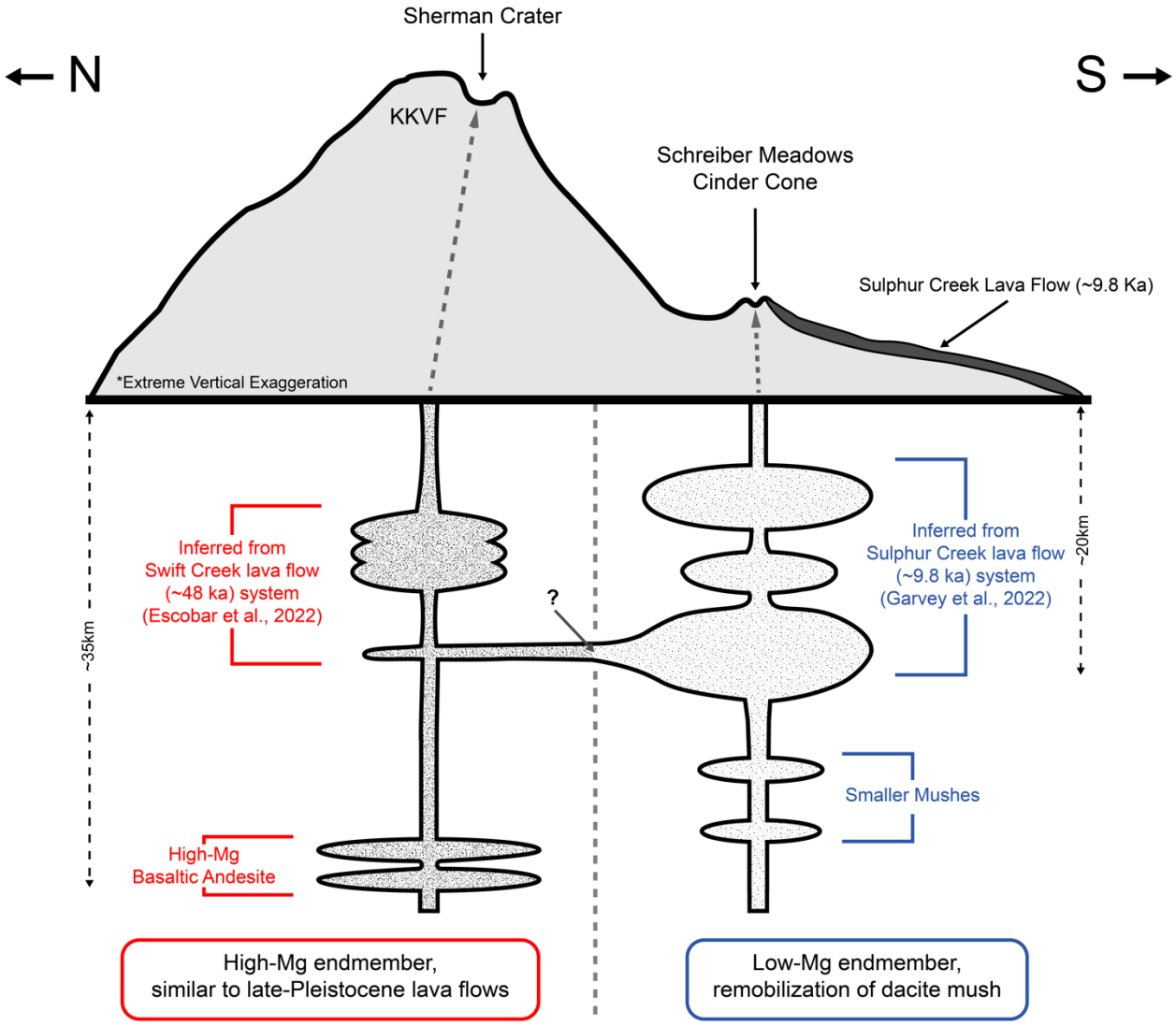

Figure 15. Cartoon model of the KKVF magma plumbing system, cross-section from north to south. The model represents the HMA/HMBA magma series feeding the main edifice (left; red) and the low-Mg calc-alkaline magma series (right; blue) feeding the southeastern flank within a 50 ka time span. The HMA/HMBA series plumbing system is derived from geobarometric estimates from Escobar (2017) and Valgardson (2022). The low-Mg calc-alkaline series is derived from geobarometric estimates of Garvey (2022). Connection between dacite mushes involved in subvent processes in these two magma series is denoted by a "?". Model is presented with extreme vertical exaggeration of the volcanic edifice.

Appendices

Appendix 1: Major Element Concentrations Data table

Sample	Label	SiO_2	TiO_2	Al_2O_3	FeO	MnO	MgO	CaO	Na_2O	K_2O	P_2O_5	Total
DT091109	Spectrum 33	69.22	0.77	15.02	3.03	0.12	0.59	1.7	4.6	4.81	0.14	100
Thunder Lakes	Spectrum 34	69.19	0.85	15.11	3.14	0.11	0.61	1.71	4.49	4.77	0.01	100
GM 2, Circle 1	Spectrum 35	70.24	0.81	15.37	3.04	0.06	0.59	1.73	3.18	4.88	0.1	100
Grain 1, Space 1	Spectrum 36	70.48	0.84	15.02	3.09	0.07	0.59	1.57	3.38	4.8	0.17	100
	Spectrum 37	70.6	0.86	15.14	3.15	0.08	0.6	1.65	3.03	4.82	0.06	100
	Spectrum 38	70.48	0.78	15.18	3.08	0.13	0.64	1.64	3.22	4.79	0.06	100
Average wt. %		**70.04**	**0.82**	**15.14**	**3.09**	**0.10**	**0.60**	**1.67**	**3.65**	**4.81**	**0.09**	**100.00**
DT072609	Spectrum 16	78.37	0.16	12.07	0.9	0.01	0.12	0.92	3.61	3.84	0	100
Ptarmigan Ridge Lapilli	Spectrum 17	78.29	0.2	12.17	0.88	0.01	0.15	0.95	3.47	3.88	0	100
GM 2, Circle 5	Spectrum 18	79.05	0.21	12.22	0.94	0.04	0.13	0.89	2.61	3.91	0	100
Grain 2, Space 2	Spectrum 19	78.84	0.23	12.41	0.89	0	0.16	0.88	2.71	3.81	0.07	100
	Spectrum 20	78.91	0.15	12.27	0.92	0.06	0.17	0.93	2.78	3.8	0	100
	Spectrum 21	78.99	0.2	12.17	0.88	0	0.17	0.96	2.72	3.92	0	100
Average wt. %		**78.74**	**0.19**	**12.22**	**0.90**	**0.02**	**0.15**	**0.92**	**2.98**	**3.86**	**0.01**	**100.00**
DT072306B	box Spectrum 1	68.88	0.8	15.2	3.07	0.01	0.57	2.01	4.79	4.55	0.13	100
Heliotrope Trail BA	box Spectrum 2	69.84	0.88	14.89	3.29	0.13	0.65	1.59	3.76	4.9	0.07	100
GM 3, Only Circle	Spectrum 3	70.23	0.89	14.68	3.27	0.07	0.57	1.5	3.74	4.9	0.16	100
Grain 1, Space 1	Spectrum 4[1]	61.4	0.24	23.23	1	0.02	0.16	5.91	6.61	1.35	0.08	100
	Spectrum 5	70.19	0.94	15.01	3.11	0.04	0.49	1.62	3.66	4.8	0.14	100
	Spectrum 6[1]	64.82	0.51	**20.13**	1.55	0.04	0.23	3.98	6.12	2.62	0	100
Average wt. %		**67.56**	**0.71**	**17.19**	**2.55**	**0.05**	**0.45**	**2.77**	**4.78**	**3.85**	**0.10**	**100.00**
DT072306B	box Spectrum 10	68.42	0.92	15.27	3.35	0.08	0.79	1.98	4.88	4.3	0.02	100

Sample	Label	SiO2	TiO2	Al2O3	FeO	MnO	MgO	CaO	Na2O	K2O	P2O5	Total
Heliotrope Trail BA	box Spectrum 11	68.55	0.82	15.21	3.3	0.11	0.77	1.74	4.82	4.67	0.01	100
GM 3, Only Circle	box Spectrum 12	68.04	0.82	15.43	3.44	0.09	0.88	2.15	5.02	4.03	0.1	100
Grain 2, Space 2	box Spectrum 13	68.36	0.84	15.18	3.35	0.12	0.73	1.5	4.66	5.19	0.06	100
	Spectrum 14	68.58	0.84	15.2	3.45	0.05	0.79	1.98	4.75	4.18	0.18	100
	Spectrum 15	69.21	0.81	15.29	3.16	0.04	0.7	2.06	4.77	3.87	0.09	100
	Spectrum 16	71.68	0.95	13.65	3.2	0.03	0.71	2.11	3.6	3.99	0.09	100
	Spectrum 17	69.03	0.8	15.59	2.97	0.07	0.58	2.15	5.06	3.75	0	100
	Spectrum 18	67.25	0.94	15.81	3.56	0.11	0.92	2.73	5.34	3.25	0.1	100
	Spectrum 19	67.91	0.81	15.94	3.3	0.07	0.72	2.4	5.23	3.51	0.11	100
	Spectrum 20	68.76	0.83	14.39	3.94	0.11	0.96	1.13	3.94	5.94	0	100
	Spectrum 21	68.4	0.76	15.18	3.25	0.05	0.77	1.12	4.14	6.27	0.06	100
Average wt. %		**68.68**	**0.85**	**15.18**	**3.36**	**0.08**	**0.78**	**1.92**	**4.68**	**4.41**	**0.07**	**100.00**
DT091109	box Spectrum 19	68.71	0.88	15.24	3.15	0.05	0.76	1.88	4.9	4.39	0.05	100
Thunder Lakes	box Spectrum 20	68.86	0.9	15.27	3.15	0.05	0.7	1.93	4.75	4.39	0	100
GM 4, Circle 1	Spectrum 21	70.04	0.92	15.13	3.27	0.13	0.76	2.06	3.4	4.18	0.11	100
Grain 1, Space 1	Spectrum 22	69.76	0.96	15.54	3.42	0.05	0.73	2.01	3.03	4.33	0.16	100
	Spectrum 23	69.85	0.9	15.4	3.32	0.05	0.78	1.94	3.53	4.18	0.03	100
	Spectrum 24	70.63	0.9	15.64	3.17	0.06	0.7	1.93	2.59	4.35	0.03	100
Average wt. %		**69.64**	**0.91**	**15.37**	**3.25**	**0.07**	**0.74**	**1.96**	**3.70**	**4.30**	**0.06**	**100.00**
BA near Sherman	box Spectrum 1	66.54	0.73	16.8	3.07	0.05	0.68	2.86	5.28	3.66	0.33	100
Sherman Crater	box Spectrum 2	66.36	0.81	17.25	3.25	0.07	0.71	2.57	4.91	4.04	0.05	100
GM 4, Circle 2	Spectrum 3	67.65	0.79	16.83	3.29	0.1	0.76	2.73	4.01	3.82	0.02	100
Grain 2, Space 2	Spectrum 4	68	0.84	16.45	3.13	0.08	0.72	2.6	4.27	3.73	0.18	100
	Spectrum 5	69.65	0.95	15.26	3.61	0.06	0.82	1.83	3.22	4.45	0.16	100
	Spectrum 6	68.3	0.88	15.47	3.66	0.08	0.83	1.99	4.13	4.51	0.16	100
Average wt. %		**67.75**	**0.83**	**16.34**	**3.34**	**0.07**	**0.75**	**2.43**	**4.30**	**4.04**	**0.15**	**100.00**
BA near Sherman	box Spectrum 7	67.36	0.85	15.92	3.42	0.04	0.85	2.32	4.91	4.26	0.07	100

Sample	Label	SiO2	TiO2	Al2O3	FeO	MnO	MgO	CaO	Na2O	K2O	P2O5	Total
Sherman Crater	box Spectrum 8	66.39	0.79	16.76	3.34	0.02	0.75	2.89	4.94	3.95	0.16	100
GM 4, Circle 2	Spectrum 9	69.55	0.93	15.62	3.79	0.05	0.79	2.19	2.39	4.43	0.25	100
Grain 2, Space 3	Spectrum 10	67.76	0.98	16	4	0.11	1.01	2.27	3.38	4.26	0.22	100
	Spectrum 11	70.14	0.92	15.42	3.77	0.08	0.83	2.04	2.15	4.5	0.14	100
	Spectrum 12	68.86	1.03	15.89	3.96	0.07	0.99	2.23	2.44	4.35	0.18	100
Average wt. %		**68.34**	**0.92**	**15.94**	**3.71**	**0.06**	**0.87**	**2.32**	**3.37**	**4.29**	**0.17**	**100.00**
DT080920	box Spectrum 13[1]	61.15	0.49	21.96	2.13	0.03	0.41	6.08	5.63	2.01	0.12	100
Damfino Lake Trail	box Spectrum 14[1]	63.92	0.8	18.59	3.08	0.08	0.66	4.31	5.24	3.17	0.14	100
GM 4, Circle 6	Spectrum 15	66.92	1.1	15.58	4.61	0.08	0.91	3.34	2.84	4.4	0.22	100
Grain 3, Space 4	Spectrum 16	67.64	0.89	15.59	3.9	0.12	1.09	2.27	3.96	4.32	0.23	100
	Spectrum 17	67.26	0.91	16.44	3.74	0.02	0.98	2.51	3.97	4.01	0.16	100
	Spectrum 18[1]	62.01	0.49	21.34	2.41	0.04	0.38	5.08	5.81	2.38	0.06	100
Average wt. %		**64.82**	**0.78**	**18.25**	**3.31**	**0.06**	**0.74**	**3.93**	**4.58**	**3.38**	**0.16**	**100.00**
DT062506	C1-G1-Spectrum 1	68.48	0.9	15.73	3.66	0.06	1	2.4	3.82	3.85	0.09	100
Gold Run Pass Trail	C1-G1-Spectrum 3 (box)	67.51	0.86	15.57	3.56	0.13	1	2.47	4.91	3.87	0.11	100
GM 5, Circle 1												
Grain 1, Space 1												
Average wt. %		**68.00**	**0.88**	**15.65**	**3.61**	**0.10**	**1.00**	**2.44**	**4.37**	**3.86**	**0.10**	**100.00**
DT062506	Spectrum 18	70.05	0.91	15.39	3.54	0.1	0.79	2.17	2.75	4.09	0.11	99.91
Gold Run Pass Trail	Spectrum 19	68.73	0.86	15.22	3.53	0.09	0.75	2.1	4.43	4.1	0.1	99.91
GM 5, Circle 1												
Grain 1, Space 2												
Average wt. %		**69.39**	**0.89**	**15.31**	**3.54**	**0.10**	**0.77**	**2.14**	**3.59**	**4.10**	**0.11**	**99.91**
DT062506	Spectrum 21	63.26	1.38	16.3	5.88	0.09	2.06	4.03	3.91	2.76	0.34	100
Gold Run Pass Trail	Spectrum 22	62.5	1.41	16.18	5.54	0.09	2.06	4.05	5.1	2.72	0.34	100
GM 5, Circle 1												
Grain 2, Space 3												

Sample	Label	SiO2	TiO2	Al2O3	FeO	MnO	MgO	CaO	Na2O	K2O	P2O5	Total
Average wt. %		**62.88**	**1.40**	**16.24**	**5.71**	**0.09**	**2.06**	**4.04**	**4.51**	**2.74**	**0.34**	**100.00**
DT082005A	Spectrum 1	70.64	0.91	14.48	3.22	0.17	0.53	1.27	3.54	4.86	0.39	100
Shuksan Lake Trail	Spectrum 2	71.15	0.94	14.33	3.2	0.02	0.5	1.28	3.36	5.17	0.04	100
GM 6, Circle 1	Spectrum 3	71.2	0.91	14.35	3.22	0.06	0.49	1.31	3.25	5.09	0.12	100
Grain 1, Space 1	Spectrum 4	71.25	0.92	14.21	3.17	0.06	0.54	1.25	3.44	4.85	0.32	100
	Spectrum 5	71.13	0.92	14.35	3.29	0.07	0.52	1.26	3.24	5.11	0.12	100
	Spectrum 6	71.24	0.94	14.39	3.22	0.03	0.49	1.29	3.27	4.98	0.14	100
Average wt. %		**71.10**	**0.92**	**14.35**	**3.22**	**0.07**	**0.51**	**1.28**	**3.35**	**5.01**	**0.19**	**100.00**
DT082005A	Spectrum 7	67.99	0.91	15.77	3.45	0.1	0.7	2.35	4.29	4.02	0.43	100
Shuksan Lake Trail	Spectrum 8	68.75	1.02	14.87	3.82	0.05	0.68	1.85	3.85	5.08	0.02	100
GM 6, Circle 1	Spectrum 9	68.58	1.06	14.61	3.89	0.04	0.79	1.84	4	5.11	0.09	100
Grain 2, Space 2	Spectrum 10	67.67	1.03	14.64	3.89	0.07	0.75	2.25	4.23	5.14	0.34	100
Average wt. %		**68.25**	**1.01**	**14.97**	**3.76**	**0.07**	**0.73**	**2.07**	**4.09**	**4.84**	**0.22**	**100.00**
DT070607A	C1G1 Spectrum 14	69.13	0.86	15.62	3.43	0.07	0.85	2.33	3.25	4.35	0.11	100
Schreibers Meadow Road	C1G1 Spectrum 15	67.9	0.79	15.62	3.31	0.12	0.89	2.33	4.65	4.28	0.11	100
GM 10, Circle 1	C1G1 Spectrum 16	68.07	0.87	15.64	3.24	0.1	0.84	2.25	4.58	4.29	0.12	100
Grain 1, Space 1												
Average wt. %		**68.37**	**0.84**	**15.63**	**3.33**	**0.10**	**0.86**	**2.30**	**4.16**	**4.31**	**0.11**	**100.00**
DT091409A	C2G1 Spectrum 7	78.82	0.3	12.31	0.92	0.04	0.2	0.93	2.62	3.86	0	100
Spoon Lake	C2G1 Spectrum 8	79.07	0.25	12.28	0.97	0.01	0.13	0.94	2.54	3.81	0	100
GM 10, Circle 2	C2G1 Spectrum 9	78.13	0.17	12.25	0.95	0.01	0.16	0.92	3.55	3.85	0	100
Grain 2, Space 2	C2G1 Spectrum 10	78.22	0.22	12.24	0.97	0.02	0.15	0.85	3.54	3.79	0	100
Average wt. %		**78.56**	**0.24**	**12.27**	**0.95**	**0.02**	**0.16**	**0.91**	**3.06**	**3.83**	**0.00**	**100.00**
DT092706C	Spectrum 18	71.3	0.75	15.44	2.42	0.04	0.59	1.35	3.81	4.25	0.06	100
Boulder Ridge	Spectrum 19	71.92	0.74	15.05	2.38	0.04	0.56	1.3	3.52	4.37	0.13	100
GM 13, Circle 2	box Spectrum 20	68.17	0.6	16.82	2.18	0.02	0.6	2.33	5.62	3.56	0.1	100
Grain 1, Space 1	box Spectrum 21	69.66	0.74	15.81	2.23	0.04	0.58	1.68	5.18	3.93	0.15	100

Sample	Label	SiO2	TiO2	Al2O3	FeO	MnO	MgO	CaO	Na2O	K2O	P2O5	Total
	Spectrum 22	68.48	0.64	17.52	1.89	0.08	0.38	2.6	5.48	2.77	0.16	100
Average wt. %		**69.91**	**0.69**	**16.13**	**2.22**	**0.04**	**0.54**	**1.85**	**4.72**	**3.78**	**0.12**	**100.00**
DT092706C	box Spectrum 1[1]	66.51	0.49	18.25	1.99	0	0.65	2.74	6.14	3.2	0.03	100
Boulder Ridge	box Spectrum 2[1]	66.22	0.55	18.25	1.93	0.08	0.67	2.81	6.22	3.25	0.03	100
GM 13, Circle 4	Spectrum 3	70.16	0.79	15.2	2.54	0.08	0.7	1.36	4.56	4.48	0.13	100
Grain 2, Space 2	Spectrum 4[1]	64.14	0.31	21.26	1.03	0.02	0.25	3.84	7.11	1.94	0.09	100
Average wt. %		**66.76**	**0.54**	**18.24**	**1.87**	**0.05**	**0.57**	**2.69**	**6.01**	**3.22**	**0.07**	**100.00**
DT092706C	box Spectrum 8	69.02	0.68	15.95	2.39	0.08	0.8	1.85	5.39	3.68	0.15	100
Boulder Ridge	Spectrum 10	71.16	0.68	15.93	2.52	0.03	0.76	1.56	3.32	3.94	0.11	100
GM 13, Circle 4	Spectrum 11	70.94	0.69	15.98	2.59	0.09	0.73	1.55	3.59	3.85	0	100
Grain 3, Space 3	Spectrum 12	70.73	0.73	16.01	2.44	0.11	0.76	1.81	3.56	3.71	0.14	100
	box Spectrum 13	69.56	0.59	15.79	2.59	0.05	0.84	1.69	5.05	3.81	0.04	100
Average wt. %		**70.28**	**0.67**	**15.93**	**2.51**	**0.07**	**0.78**	**1.69**	**4.18**	**3.80**	**0.09**	**100.00**
DT091407A	C1G1 spectrum 2	78.42	0.19	12.23	0.84	0	0.16	0.78	3.03	3.17	0.1	98.93
Cow Heaven Trail	C1G1 spectrum 3	77.88	0.16	12.34	0.87	0.06	0.21	0.94	3.66	3.77	0	99.89
GM 14, Circle 1	C1G1 spectrum 4	78.2	0.21	12.14	0.88	0.02	0.17	0.88	3.56	3.8	0	99.85
Grain 1, Space 1												
Average wt. %		**78.17**	**0.19**	**12.24**	**0.86**	**0.03**	**0.18**	**0.87**	**3.42**	**3.58**	**0.03**	**99.56**
DT090797(=MB578)	C6G1 spectrum 9	62.4	1.17	16.71	5.11	0.1	2.47	4.95	4.58	2.21	0.29	100
Cow Heaven Trail	C6G1 spectrum 10	62.56	1.16	16.89	5.28	0.12	2.58	5.09	4.02	2.1	0.21	100
GM 14, Circle 6	C6G1 spectrum 11	63.03	1.22	16.84	5.02	0.05	2.48	4.88	3.99	2.21	0.27	100
Grain 2, Space 2	C6G1 spectrum 12	63.18	1.19	16.85	4.9	0.1	2.52	4.78	4.03	2.27	0.19	100
Average wt. %		**62.79**	**1.19**	**16.82**	**5.08**	**0.09**	**2.51**	**4.93**	**4.16**	**2.20**	**0.24**	**100.00**
DT072306B	box Spectrum 7	70.14	0.62	15.63	2.75	0.13	0.75	1.52	3.99	4.32	0.15	100
Heliotrope Trail	Spectrum 8	70.73	0.71	15.71	2.69	0.04	0.76	1.46	3.62	4.22	0.06	100
GM 16, Circle 3	Spectrum 9	70.56	0.62	15.61	2.74	0.02	0.78	1.51	3.75	4.31	0.09	100
Grain 1, Space 1	Spectrum 10	69.87	0.69	15.4	2.63	0.03	0.73	1.51	4.71	4.39	0.04	100

Sample	Label	SiO2	TiO2	Al2O3	FeO	MnO	MgO	CaO	Na2O	K2O	P2O5	Total
	box Spectrum 11	69.93	0.7	15.31	2.61	0.09	0.7	1.47	4.81	4.37	0	100
Average wt. %		**70.25**	**0.67**	**15.53**	**2.68**	**0.06**	**0.74**	**1.49**	**4.18**	**4.32**	**0.07**	**100.00**
DT081105C	box Spectrum 16	78	0.23	12.56	0.86	0	0.12	0.88	4.02	3.32	0	100
Park Butte	box Spectrum 17	78	0.2	12.42	0.87	0.03	0.19	0.95	3.9	3.45	0	100
GM 16, Circle 4	Spectrum 18	75.19	0.36	13.85	2.36	0	0.22	1.37	2.21	3.41	1.02	100
Grain 2, Space 2	Spectrum 19	79.13	0.23	12.41	0.89	0.04	0.14	0.89	2.84	3.44	0	100
	Spectrum 20	73.59	0.78	13.15	2.44	0.02	0.19	2.57	2.05	3.66	1.55	100
	Spectrum 24	78.86	0.23	12.43	0.9	0.01	0.22	0.91	2.84	3.61	0	100
	Spectrum 25	78.94	0.16	12.54	0.84	0.01	0.16	0.94	2.89	3.5	0	100
	Spectrum 26	79.01	0.19	12.53	0.92	0.04	0.17	0.86	2.84	3.45	0	100
Average wt. %		**77.59**	**0.30**	**12.74**	**1.26**	**0.02**	**0.18**	**1.17**	**2.95**	**3.48**	**0.32**	**100.00**
DT072609	box Spectrum 4	69.03	0.88	15.17	3.28	0.04	0.49	1.55	4.72	4.8	0.04	100
Surface of Ptarmigan Ridge	box Spectrum 5	69.43	0.9	14.81	3.47	0.11	0.55	1.34	4.25	5.11	0.04	100
GM 17, Only	box Spectrum 6	69.25	0.77	15.27	3.1	0.07	0.48	1.59	4.77	4.69	0.01	100
Grain 1, Space 1	Spectrum 7	70.55	0.86	15.04	3.21	0.12	0.64	1.24	3.41	4.84	0.08	100
	Spectrum 8	70.86	0.91	15.38	2.7	0.07	0.59	1.77	3.32	4.3	0.1	100
	Spectrum 9	70.97	0.86	14.72	3.14	0.08	0.6	1.72	3.67	4.09	0.15	100
	Spectrum 10	70.6	0.91	14.86	3.85	0.05	0.56	1.15	3.04	4.86	0.13	100
	Spectrum 11	70.41	0.87	15.31	3.6	0.07	0.58	1.2	2.9	5.06	0	100
Average wt. %		**70.14**	**0.87**	**15.07**	**3.29**	**0.08**	**0.56**	**1.45**	**3.76**	**4.72**	**0.07**	**100.00**
DT072609	box Spectrum 13	68.83	0.78	15.47	3.08	0	0.59	1.89	4.68	4.68	0	100
Surface of Ptarmigan Ridge	box Spectrum 14	68.97	0.73	15.84	2.84	0.07	0.45	1.99	4.64	4.46	0	100
GM 17, Only	box Spectrum 15	69.03	0.74	15.35	3.04	0.1	0.65	1.8	4.57	4.72	0	100
Grain 1, Space 2	Spectrum 16	70.27	0.8	15.48	3.31	0.04	0.55	1.3	3.16	5.06	0.03	100
	Spectrum 17	69.22	0.61	16.52	2.31	0.03	0.51	2.82	4.92	3.03	0.02	100
	Spectrum 18	70.6	0.81	14.99	3.2	0.08	0.5	1.45	3.16	5.17	0.04	100
	Spectrum 19	72.11	0.87	14.95	3.79	0.09	0.65	1.56	1.47	4.46	0.07	100

Sample	Label	SiO2	TiO2	Al2O3	FeO	MnO	MgO	CaO	Na2O	K2O	P2O5	Total
Average wt. %		**69.86**	**0.76**	**15.51**	**3.08**	**0.06**	**0.56**	**1.83**	**3.80**	**4.51**	**0.02**	**100.00**
22KK-BAt-02b Scott Paul Trail GM 19, Circle 3 Grain 1, Space 1	Spectrum 17	67.64	1.03	15.42	3.43	0.09	0.84	2.02	5.17	4.21	0.16	100
Average wt. %		**67.64**	**1.03**	**15.42**	**3.43**	**0.09**	**0.84**	**2.02**	**5.17**	**4.21**	**0.16**	**100**
22KK-BAt-02b Scott Paul Trail GM 19, Circle 4 Grain 2, Space 2	Spectrum 18	69.61	0.98	15.52	2.57	0.16	0.71	1.89	5.46	3.11	0	100
Average wt. %		**69.61**	**0.98**	**15.52**	**2.57**	**0.16**	**0.71**	**1.89**	**5.46**	**3.11**	**0**	**100**
DT092706C Boulder Ridge GM 19, Circle 6 Grain 3, Space 3	Spectrum 14	67.78	0.81	15.6	3.09	0.1	0.85	2.04	5.24	4.21	0.27	100
Average wt. %		**67.78**	**0.81**	**15.6**	**3.09**	**0.1**	**0.85**	**2.04**	**5.24**	**4.21**	**0.27**	**100**
DT091407A	box Spectrum 5	75.57	0.19	13.86	0.83	0.04	0.14	1.74	3.9	3.73	0	100
Cow Heaven Trail	box Spectrum 6	77.79	0.21	12.43	0.88	0.02	0.13	0.87	3.37	4.29	0	100
GM 20, Circle 4	Spectrum 7	78.66	0.2	12.15	0.86	0.08	0.08	0.78	2.67	4.52	0	100
Grain 1, Space 1	Spectrum 8	78.6	0.27	12.16	0.88	0.02	0.15	0.8	2.83	4.29	0	100
	Spectrum 9	78.61	0.19	12.23	0.91	0.04	0.12	0.78	2.76	4.37	0	100
	Spectrum 10	78.35	0.21	12.12	0.96	0.06	0.21	0.83	2.81	4.45	0	100
Average wt. %		**77.93**	**0.21**	**12.49**	**0.89**	**0.04**	**0.14**	**0.97**	**3.06**	**4.28**	**0.00**	**100.00**
DT091407A	box Spectrum 18	77.85	0.2	12.39	0.92	0.06	0.21	0.98	3.61	3.77	0	100
Cow Heaven Trail	box Spectrum 19	77.79	0.23	12.31	0.95	0.06	0.21	1.01	3.69	3.75	0	100
GM 20, Circle 4	Spectrum 20	78.86	0.17	12.5	0.85	0.01	0.21	0.93	2.74	3.7	0.03	100
Grain 2, Space 2	Spectrum 21	78.97	0.23	12.38	0.95	0	0.19	0.99	2.59	3.71	0	100

Sample	Label	SiO2	TiO2	Al2O3	FeO	MnO	MgO	CaO	Na2O	K2O	P2O5	Total
	Spectrum 22	78.78	0.19	12.47	0.89	0.05	0.2	0.98	2.74	3.7	0	100
	Spectrum 23	78.79	0.21	12.47	0.89	0.05	0.18	0.94	2.71	3.76	0	100
Average wt. %		**78.51**	**0.21**	**12.42**	**0.91**	**0.04**	**0.20**	**0.97**	**3.01**	**3.73**	**0.01**	**100.00**
DT091407A	box Spectrum 24	77.75	0.27	12.37	0.95	0	0.19	0.99	3.66	3.83	0	100
Cow Heaven Trail	box Spectrum 25	78.11	0.21	12.27	0.9	0	0.14	0.95	3.61	3.81	0	100
GM 20, Circle 4	Spectrum 26	78.67	0.25	12.45	1.01	0.12	0.15	0.98	2.69	3.67	0	100
Grain 2, Space 3	Spectrum 27	78.92	0.2	12.44	0.89	0.01	0.17	0.97	2.66	3.73	0	100
	Spectrum 28	78.84	0.2	12.45	1	0	0.18	0.99	2.57	3.77	0	100
	Spectrum 29	78.66	0.27	12.47	0.99	0.06	0.21	0.96	2.65	3.74	0	100
Average wt. %		**78.49**	**0.23**	**12.41**	**0.96**	**0.03**	**0.17**	**0.97**	**2.97**	**3.76**	**0.00**	**100.00**
DT072306B	box Spectrum 11	65.95	0.85	14.96	6.75	0	0.84	1.67	5.15	3.81	0.02	100
Heliotrope Trail	box Spectrum 12	65.59	0.71	15.03	7.31	0	0.8	1.66	5.04	3.87	0	100
GM 21, Circle 2	Spectrum 13	66.86	0.67	15.15	8.06	0	0.78	1.63	3.03	3.65	0.17	100
Grain 1, Space 1	Spectrum 14	68.07	0.7	15.21	6.68	0	0.86	1.7	2.96	3.72	0.11	100
	Spectrum 15	67.36	0.73	15.32	7.33	0	0.82	1.79	2.93	3.71	0	100
Average wt. %		**66.77**	**0.73**	**15.13**	**7.23**	**0.00**	**0.82**	**1.69**	**3.82**	**3.75**	**0.06**	**100.00**
DT072306B	box Spectrum 16	65.5	0.69	15.06	7.04	0	0.92	1.73	5.1	3.95	0.02	100
Heliotrope Trail	b0x Spectrum 17	65.25	0.56	14.78	7.66	0	1.1	1.7	5.01	3.84	0.11	100
GM 21, Circle 2	Spectrum 18	68.46	0.87	15.56	7.06	0	0.78	1.57	2.13	3.34	0.23	100
Grain 1, Space 2	Spectrum 19	66.91	0.62	15.45	9.85	0	0.82	1.36	2.2	2.79	0	100
	Spectrum 20	67.55	0.5	15.75	8.78	0	0.92	1.43	2.24	2.83	0	100
	Spectrum 21	68.43	0.48	15.7	8.5	0	0.74	1.37	1.95	2.83	0	100
Average wt. %		**67.02**	**0.62**	**15.38**	**8.15**	**0.00**	**0.88**	**1.53**	**3.11**	**3.26**	**0.06**	**100.00**
HLGPush1_BA_A[2]	box Spectrum 23	67.54	0.96	15.82	3.41	0.01	0.74	2.06	4.89	4.57	0	100
Highwood Lake	Spectrum 24	68.09	0.9	15.18	3.61	0.02	0.86	1.82	4.6	4.92	0	100
GM 25, Circle 2	Spectrum 25	65.8	0.51	18.67	2.22	0.02	0.42	3.09	6.04	3.23	0	100
Grain 1, Space 1	Spectrum 26	68.39	0.87	15.15	3.46	0.07	0.72	1.66	4.59	5.08	0	100

Sample	Label	SiO2	TiO2	Al2O3	FeO	MnO	MgO	CaO	Na2O	K2O	P2O5	Total
	Spectrum 27	66.43	0.85	17.15	3.11	0	0.55	2.95	5	3.96	0	100
	Spectrum 29	64.38	0.49	20.18	2.02	0	0.31	4.31	5.75	2.57	0	100
	box Spectrum 31	67.03	0.75	16.23	3.32	0.06	0.74	2.55	4.94	4.38	0	100
Average wt. %		**66.81**	**0.76**	**16.91**	**3.02**	**0.03**	**0.62**	**2.63**	**5.12**	**4.10**	**0.00**	**100.00**
HLGPush1_BA_A2*[2]	box Spectrum 35[1]	65.88	0.71	18.23	2.51	0.07	0.46	3.45	5.06	3.66	0	100
Highwood Lake	box Spectrum 36	67.57	0.82	16.12	3.15	0.05	0.55	2.31	4.85	4.58	0	100
GM 25, Circle 6	Spectrum 39	59.04	0.14	25.22	0.93	0	0.16	7.44	6.12	0.96	0	100
Grain 2, Space 2	Spectrum 40	68.34	0.88	15.81	3.2	0.11	0.56	2.41	4.14	4.56	0	100
	Spectrum 41	68.71	0.86	15.49	3.36	0	0.67	1.97	4.05	4.89	0	100
	Spectrum 42	69.32	0.92	14.96	3.43	0.08	0.66	1.58	3.89	5.17	0	100
	Spectrum 43	67.44	0.81	17.08	2.66	0.02	0.57	3.32	4.2	3.81	0	99.91
	Spectrum 46	69.3	1.01	14.96	3.46	0	0.54	1.66	3.94	5.13	0	100
Average wt. %		**66.95**	**0.77**	**17.23**	**2.84**	**0.04**	**0.52**	**3.02**	**4.53**	**4.10**	**0.00**	**99.99**
HLGPush1_BA_A2*[2]	box Spectrum 52	66.87	0.8	15.78	3.78	0.04	0.98	2.42	4.84	4.49	0	100
Highwood Lake	Spectrum 57	68.24	0.9	15.29	3.81	0.06	0.7	1.67	4.33	5.02	0	100
GM 25, Circle 6	Spectrum 58[1]	62.92	0.49	21.13	1.96	0	0.29	5.07	5.95	2.19	0	100
Grain 3, Space 3	Spectrum 59[1]	62.42	0.44	21.53	1.94	0.08	0.32	5.34	5.7	2.23	0	100
	box Spectrum 60	68.09	0.94	15.24	3.62	0.05	0.68	1.77	4.63	4.99	0	100
	Spectrum 63	68.75	0.91	15.09	3.59	0	0.66	1.53	4.35	5.11	0	100
Average wt. %		**66.22**	**0.75**	**17.34**	**3.12**	**0.04**	**0.61**	**2.97**	**4.97**	**4.01**	**0.00**	**100.00**
HLGPush1_BA_B[2]	Spectrum 2	68.67	0.96	14.95	3.62	0.05	0.57	1.54	4.43	5.21	0	100
Highwood Lake	Spectrum 3[1]	66.57	0.69	17.71	2.69	0.07	0.37	3.03	4.94	3.93	0	100
GM 26, Circle 3	Spectrum 4	69.59	0.97	15.14	3.38	0.09	0.59	1.46	3.45	5.27	0.05	100
Grain 1, Space 1	Spectrum 5	69.81	0.94	14.99	3.48	0.11	0.58	1.62	3.24	5.18	0.06	100
	Spectrum 6	70.08	0.96	14.8	3.54	0	0.61	1.54	3.24	5.16	0.09	100
	Spectrum 7	69.72	1.02	15.12	3.54	0.11	0.51	1.37	3.33	5.23	0.05	100
Average wt. %		**69.07**	**0.92**	**15.45**	**3.38**	**0.07**	**0.54**	**1.76**	**3.77**	**5.00**	**0.04**	**100.00**

Sample	Label	SiO2	TiO2	Al2O3	FeO	MnO	MgO	CaO	Na2O	K2O	P2O5	Total
HLGPush1_BA_B[2]	Spectrum 13	69.21	1.19	14.57	3.18	0.06	0.56	1.31	4.74	5.16	0	100
Highwood Lake	Spectrum 14	68.77	1.15	15.16	3.3	0.04	0.54	1.62	4.45	4.97	0	100
GM 26, Circle 3	Spectrum 15	71.16	1.34	15.05	3.5	0.07	0.59	1.38	1.96	4.89	0.06	100
Grain 2, Space 2	Spectrum 16	69.92	1.26	14.7	3.42	0.06	0.57	1.39	3.52	5.12	0.04	100
	Spectrum 17	70.81	1.28	15.21	3.65	0.11	0.56	1.48	2.06	4.78	0.06	100
	Spectrum 19	72.57	1.3	15.21	3.59	0.04	0.56	1.34	1.15	4.23	0.01	100
Average wt. %		**70.41**	**1.25**	**14.98**	**3.44**	**0.06**	**0.56**	**1.42**	**2.98**	**4.86**	**0.03**	**100.00**
HLGPush1_BA_C[2]	Spectrum 20	68.69	0.76	15.58	2.87	0.04	0.47	1.92	4.88	4.78	0	100
Highwood Lake	Spectrum 21	67.57	0.7	16.87	2.61	0.06	0.41	2.62	4.98	4.17	0	100
GM 26, Circle 4	Spectrum 22	68.28	0.7	15.91	2.8	0.03	0.54	2.34	4.79	4.52	0.09	100
Grain 3, Space 3	Spectrum 23	70.51	0.81	14.65	3.29	0.03	0.54	1.35	3.66	5.17	0	100
	Spectrum 24[1]	64.16	0.32	21.49	1.47	0.06	0.2	5.01	4.96	2.31	0.02	100
	Spectrum 25	70.48	0.8	14.81	3.06	0.01	0.54	1.34	3.67	5.28	0	100
	Spectrum 26	70.99	0.89	14.58	3.08	0.12	0.52	1.26	3.27	5.29	0	100
Average wt. %		68.67	0.71	16.27	2.74	0.05	0.46	2.26	4.32	4.50	0.02	100.00
HLGPush1_BA_C[2]	box Spectrum 27	67.82	0.78	16.08	3.09	0.06	0.59	2.34	4.89	4.35	0	100
Highwood Lake	box Spectrum 28	68.28	0.96	15.23	3.26	0.13	0.64	1.91	4.71	4.79	0.09	100
GM 26, Circle 4	Spectrum 29[1]	60.42	0.19	23.77	1.23	0.05	0.28	6.16	6.45	1.44	0	100
Grain 4, Space 4	Spectrum 30	71.37	0.94	15.28	3.48	0.07	0.64	1.66	1.71	4.79	0.04	100
	Spectrum 31	69.61	0.95	15.07	3.37	0.04	0.62	1.67	3.61	5.01	0.05	100
	Spectrum 32	69.83	1	14.97	3.43	0.08	0.63	1.72	3.34	4.91	0.1	100
	Spectrum 33[1]	61.48	0.27	23.37	0.97	0	0.16	6.11	6.18	1.46	0	100
Average wt. %		66.97	0.73	17.68	2.69	0.06	0.51	3.08	4.41	3.82	0.04	100.00
HLGPush1_BA_C[2]	box Spectrum 34	65.27	0.81	17.33	3.4	0.1	0.89	3.4	4.98	3.65	0.18	100
Highwood Lake	box Spectrum 35	65.24	0.81	17.29	3.58	0.07	1.03	3.6	4.8	3.52	0.07	100
GM 26, Circle 4	Spectrum 36	67.53	0.89	15.81	4.13	0.12	1.13	2.53	3.24	4.42	0.2	100
Grain 5, Space 5	Spectrum 37[1]	64.34	0.53	20.31	2.25	0.05	0.69	4.74	4.56	2.52	0	100

Sample	Label	SiO2	TiO2	Al2O3	FeO	MnO	MgO	CaO	Na2O	K2O	P2O5	Total
	Spectrum 38	60.63	0.32	23.09	1.66	0.02	0.39	6.43	5.96	1.5	0	100
	Spectrum 39	67.2	0.97	16.04	4.15	0.1	1.1	2.46	3.38	4.4	0.2	100
	Spectrum 40	67.46	1.04	15.83	4.21	0.11	1.02	2.44	3.52	4.16	0.2	100
Average wt. %		65.38	0.77	17.96	3.34	0.08	0.89	3.66	4.35	3.45	0.12	100.00
MB-651a[3] Sherman Crater	XRF lapillus	57.9	1.03	17.04	6.51		4.31	6.78	3.96	1.62		98.21

[1] Analyses that accidentally include a significant proportion of plagioclase microlites. These analyses are not included in the average.
[2] Samples HLGPush1_BA_A, HLGPush1_BA_ A2, HLGPush1_BA_A2*, HLGPush1_BA_B, and HLGPush1_BA_C simplified to "HLGPush1_BA" in Figures 2, 4-11, and 13.
[3] XRF analyses from Hildreth, 2003; analyses represented in Scott, 2020, Appendix 5, p.151.

Appendix 2: Trace Element Concentrations Data table

Element	GSD-1	GSD-2	GSD-3	GSE-1	GSE-2	GSE-3	BHVO2-1	BHVO2-2	BHVO2-3
Na23	28082.3	28203.89	28977.44	30251.83	30530.72	30205.57	17600.24	17492.48	17675.2
Mg25	21412.6	21564.92	21731.38	21205.15	21573.72	21324.06	45228.75	45045.16	45315.45
Al27	72500.01	72500.02	72500	70913.02	70913.01	70913.02	71971	71971.01	71971.01
Si29	244573.23	244190.95	250475.67	244579.03	245237.16	242184.97	235408.25	234200.72	234399.97
K39	24897.85	25059.26	25539.95	21564.46	21810.08	21485.84	4278.25	4242.61	4264.13
Ca43	51052.02	51571.77	51500.35	52945.29	53354.06	53114.66	82244.8	81936.25	82180.45
Sc45	52.24	53.29	52.94	542.88	542.21	542.66	32.65	32.47	32.79
Ti47	7693.9	7784.26	7904.89	448.23	442.25	454.73	16660.18	16623.62	16697.99
Cr53	<0.00	<0.00	<0.00	<0.00	<0.00	<0.00	<0.00	<0.00	<0.00
Fe57	103051.55	102447.36	105024.32	100309.88	101531.84	100129.65	93993.48	94186.78	94354.02
Ni60	56.94	54.87	57.5	421.45	432	420.86	121.13	120.09	123.16
Rb85	37.15	37.66	39.28	372.16	376	370.46	9.62	9.52	9.57
Sr88	68.55	69.84	69.08	452.86	458.27	454.96	396.62	397.7	395.88
Y89	44.39	45.13	45.07	456.34	458.37	456.57	26.44	26.46	26.1
Zr90	44.24	44.42	45.16	437.75	438.89	437.27	175.21	175.57	174.95
Nb93	45.54	45.54	47.04	470.58	476.77	470.14	18.91	18.77	18.85
Cs133	31.82	31.89	33.26	310.64	316.43	312.75	0.1	0.109	0.102
Ba137	69.92	67.53	69.88	440.47	443.23	442.48	134.73	134.79	131.88
La139	39.32	39.87	40.28	407.51	413.6	411.53	15.71	15.77	15.49
Ce140	40.55	41.03	41.2	420.16	426.67	422.85	37.23	37.63	37.86
Pr141	45.44	46.07	46.03	481.91	487.65	483.7	5.18	5.26	5.2
Nd146	43.86	46.03	43.53	468.04	475.11	471.28	24.48	24.85	24.8
Sm147	46.63	47.73	48.42	495.57	503.46	498.71	5.64	6.09	6.17
Eu153	39.69	41.32	40.85	416.4	424.01	419.38	1.981	2.09	2.001

Gd157	49.05	50.02	50.69	529.77	536.43	533.5	6.48	6.33	6.34
Tb159	48.36	49.63	50.2	521.69	528.18	523.22	0.942	0.962	1.002
Dy163	51.45	53.98	53.6	553.27	553.49	550.21	5.66	5.16	5.34
Ho165	49.99	50.9	51.62	527.28	532.85	533.6	1.007	0.946	1.015
Er166	38.53	39.85	40.25	618.82	618.39	619.04	2.5	2.59	2.66
Tm169	50.97	51.97	51.88	537.16	540.73	540.64	0.33	0.315	0.335
Yb171	52.25	54.06	52.79	554.11	552.1	556.01	2.27	2.07	2.03
Lu175	53.91	54.59	54.59	559.03	563.03	564.71	0.297	0.289	0.293
Hf178	39.67	41	41.34	419.12	423.75	422.31	4.35	4.53	4.75
Ta181	43.35	43.84	45.05	455.7	454.27	456.46	1.106	1.18	1.131
Pb206	49.42	51.11	52.54	400.82	409.07	406.59	2.18	1.95	2.01
Pb207	49.69	51.41	52.02	399.8	409.52	408.07	1.9	2.11	2.08
Pb208	49.67	50.84	51.95	397.98	410.06	409.74	2.14	2.03	2.11
Th232	42.19	43.38	44.11	407.37	416.77	416.09	1.28	1.358	1.304
U238	39.28	40.13	41.2	414.58	418.58	415.1	0.452	0.387	0.403

Element	06-1-01_DT082005A-1	06-1-01_DT082005A-2	06-1-02_DT082005A-1	03-1-02_DT072306B-1	03-1-02_DT072306B-2	03-1-01_DT072306B-1
Na23	35288.53	34524.32	35120.02	38006.95	38069.38	41680.02
Mg25	5135.29	5969.78	3301.55	4277.07	4510.16	4148.12
Al27	75947.43	75947.43	79228.78	80340.21	80340.21	90978.14
Si29	285021.13	276827.78	304804.91	320239.81	315007.09	345616.88
K39	30370.6	28589.57	42905.49	38607.28	36314.56	40279.71
Ca43	16009.44	18206	8544.56	12594.77	12507.78	15605.24
Sc45	7.53	7.24	9.25	9.27	8.43	9.64
Ti47	4001.07	3607.95	4307.38	4720.81	4726.1	5751.32
Cr53	<0.00	<0.00	<0.00	<0.00	<0.00	<0.00
Fe57	25105.85	23551.38	27488.33	27190.42	27518.24	29620.21
Ni60	1.4	1.16	1.01	<0.49	1.14	1.01
Rb85	75.69	70.94	116.98	86.88	85.96	105.56
Sr88	347.82	453.9	80.44	177.29	181.18	275.33
Y89	30.07	30.1	39.4	35.16	36.03	44.25
Zr90	393.55	365.76	463.74	441.11	451.27	557.1
Nb93	21.45	20.17	24.8	25.45	25.46	30.04
Cs133	2.14	1.974	3.12	2.5	2.42	3.16
Ba137	876.72	852.22	867.95	1056.36	1034.11	1061.6
La139	32.94	31.9	37.32	34.58	35.61	45.52
Ce140	67.87	66.19	75.67	72.45	73.16	94.01
Pr141	7.78	7.75	9.08	8.32	8.69	11.32
Nd146	30.34	30.26	34.15	31.54	32.93	43.69
Sm147	5.59	4.95	6.44	6.54	6.5	8.1
Eu153	1.154	1.097	0.906	1.129	1.128	1.46
Gd157	5.41	4.92	6.41	6.16	5.51	7.06
Tb159	0.764	0.784	1.062	0.911	0.92	1.233
Dy163	4.9	4.99	6.35	6.61	6.03	6.89
Ho165	1.042	0.96	1.382	1.335	1.253	1.424

Er166	3.17	2.71	3.92	3.99	3.79	4.23
Tm169	0.474	0.407	0.631	0.579	0.593	0.627
Yb171	3.34	3.37	4.18	3.75	3.67	4.92
Lu175	0.487	0.506	0.764	0.649	0.631	0.709
Hf178	9.08	8.21	10.51	9.98	10.33	12.6
Ta181	1.303	1.26	1.552	1.427	1.606	1.75
Pb206	13.07	12.4	19.53	16.84	16.82	17.54
Pb207	13.1	12.89	19.77	16.07	18.33	18.87
Pb208	14.02	12.77	19.5	16.13	17.68	18.51
Th232	10.76	10.5	13.13	11.8	12.49	15.66
U238	4.09	3.81	4.65	4.81	4.71	5.9

Element	05-1-01_DT062506-1	05-1-02_DT062506-1	05-1-03_DT062506-1	10-1-01_DT070607A-1	10-2-02_DT091409A-1	13-1-01_DT092706C-1
Na23	36643.84	37440.1	40355.17	37347.24	27020.74	41087.74
Mg25	5886.8	4726.65	12104.21	4981.64	891.52	3919.83
Al27	82827.7	81028.23	85950.27	82721.84	64939.03	85368.08
Si29	294127.13	305184.78	289520.84	306252.66	340923.38	339498.03
K39	30521.19	32276.58	22251.56	34048.73	28393.63	38133.82
Ca43	18141.56	15765.18	30153.59	16135.44	6850.55	13956.26
Sc45	9.92	9.97	16.98	9.03	2.46	8.01
Ti47	4909.83	4890.9	8256.94	5110.41	1317.72	5315.97
Cr53	<0.00	<0.00	<0.00	<0.00	<0.00	<0.00
Fe57	30613.42	29825.46	50169.89	29932.45	7744.74	29778.61
Ni60	1.68	<0.55	3.64	0.8	<0.95	<0.93
Rb85	79.24	85.99	53.06	86.61	73.18	97.53
Sr88	268.02	222.48	370.8	315.06	129.99	262.59
Y89	37.13	38.84	42.28	36.89	12.12	39.66
Zr90	428.17	448.46	389.86	438.86	135.87	493.37
Nb93	21.85	24.9	15.5	24.41	6.35	27.99
Cs133	2.44	2.52	1.518	2.48	3.15	2.76
Ba137	867.66	920.93	691.86	948.5	803.54	1048.73
La139	34.86	35.73	30.41	37.5	21.35	41.17
Ce140	69.25	72.61	67.05	76.81	39.44	86.23
Pr141	8.23	8.72	8.77	9.31	4.42	10.69
Nd146	30.42	32.69	34.14	35.81	13.76	41.8
Sm147	7.07	6.44	7.5	7.31	2.64	6.79
Eu153	1.34	1.247	1.94	1.235	0.381	1.16
Gd157	5.51	6.39	7.09	6.15	1.69	5.46
Tb159	0.908	1.041	1.139	1.008	0.355	1.024
Dy163	6.08	6.05	7.2	6.3	1.9	6.83
Ho165	1.253	1.311	1.428	1.285	0.353	1.29

Er166	3.37	3.96	4.1	3.58	1.25	4.06
Tm169	0.537	0.655	0.653	0.606	0.221	0.605
Yb171	3.56	3.64	4.39	4.55	1.6	4.08
Lu175	0.581	0.658	0.662	0.672	0.222	0.664
Hf178	9.12	10.72	8.51	9.97	3.8	11.43
Ta181	1.287	1.505	1.018	1.395	0.68	1.6
Pb206	14.35	13.76	10.31	15.32	14.5	14.28
Pb207	14.46	13.59	10.69	16.75	15.18	16.07
Pb208	13.31	14.51	10.31	15.89	15.27	16.62
Th232	10.88	12.34	7.3	11.79	11.46	13.62
U238	4.45	4.59	3.02	4.49	3.77	5.37

Element	13-4-02_DT092706C-1	13-4-03_DT092706C-1	14-1-01_DT091407A-1	14-6-02_DT090797-1	16-3-01_DT072306B-1
Na23	44073.3	40478.27	26548.73	35656	29072.74
Mg25	4246.27	4772.34	905.1	15261.69	309.27
Al27	96535.27	84309.59	64780.25	89019.91	82192.59
Si29	333409.94	332266.88	330274.47	294471.44	172586.47
K39	37106.74	36730.9	29058.43	18620.6	4711.89
Ca43	20958.04	14712.36	5840.27	38565.43	34632.33
Sc45	6.95	9.19	1.79	15.18	0.41
Ti47	4884.54	5035.8	1126.31	7137.45	417.94
Cr53	<0.00	<0.00	<0.00	<0.00	<0.00
Fe57	28117.13	30854.38	7041.56	49597.76	3644.2
Ni60	1.1	1.01	<0.80	23.7	<0.65
Rb85	90.54	95.39	71.3	35.99	6.66
Sr88	647.63	250.03	125.56	711	648.43
Y89	33.35	39.22	10.68	24.28	1.73
Zr90	451.49	476.16	120.43	230.64	22.32
Nb93	25.79	26.54	6.61	8.95	1.51
Cs133	2.64	2.72	3.34	0.889	0.118
Ba137	1106.58	1010.13	775.98	631.93	349.35
La139	38.47	39.55	19.52	22.95	5.13
Ce140	79.7	81.5	38.41	50.59	8.1
Pr141	9.6	9.61	4.22	6.5	0.814
Nd146	35.58	35.95	12.77	26.39	2.7
Sm147	5.99	7.18	1.66	5.06	0.51
Eu153	1.46	1.25	0.439	1.485	1.31
Gd157	4.66	6.61	1.98	4.66	0.388
Tb159	0.862	1.073	0.295	0.715	0.058
Dy163	5.43	6.88	2.03	4.27	0.253
Ho165	1.238	1.331	0.38	0.811	0.071

Er166	3.45	3.74	0.97	2.65	0.175
Tm169	0.538	0.599	0.163	0.338	0.0204
Yb171	4.03	4.56	1.49	2.7	0.12
Lu175	0.621	0.669	0.197	0.383	0.0254
Hf178	10.48	10.91	3.33	5.77	0.403
Ta181	1.55	1.589	0.561	0.578	0.085
Pb206	17.66	15.2	14.31	8.75	2.78
Pb207	20.76	15.53	14.87	9.5	3.01
Pb208	17.68	15.83	15.1	8.98	3.12
Th232	11.96	12.4	11.49	4.72	0.534
U238	4.68	4.77	3.74	1.83	0.283

Element	GSD-4	GSD-5	GSD-6	GSE-4	GSE-5	GSE-6	BHVO2-4	BHVO2-5	BHVO2-6
Na23	28226.5	28292.43	28459.08	30427.46	30395.89	30385.27	17712.99	17689.64	17572.95
Mg25	21594.54	21717.2	21697.12	21502.26	21219.38	21365.13	45386.55	45278.05	44774.52
Al27	72500	72500	72500	70913	70913	70913	71971	71970.99	71970.99
Si29	243475.14	244130.67	246536.09	243177.67	243397.7	245440.06	234534.94	235312.61	233539.94
K39	25050.06	24905.16	25033.62	21550.45	21466.72	21539	4280.33	4307.33	4238.95
Ca43	51784.9	51624.46	52027.78	52037.45	52704.2	53172.91	83058.77	82468.34	82101.45
Sc45	52.93	53.51	53.53	539	536.2	541.56	32.93	33.21	32.62
Ti47	7815.11	7795.71	7837.76	446.35	448.87	447.94	16496.99	16559.36	16436.33
Cr53	<0.00	<0.00	<0.00	<0.00	<0.00	<0.00	<0.00	<0.00	<0.00
Fe57	103128.57	103781.9	103568.05	100137.84	100189.48	101099.24	93141.54	93270.76	92378.8
Ni60	56.6	57.14	56.74	422.79	425.09	428.79	120.94	120.35	121.05
Rb85	37.98	38.66	38.06	368.04	368.97	369.84	9.51	9.63	9.38
Sr88	69.64	70.72	69.8	454.53	454.02	456.86	394.26	394.68	394.42
Y89	45.2	45.3	45.29	453.99	458.01	461.18	26.4	26.84	26.13
Zr90	44.83	44.1	45.2	435.78	433.86	437.56	176.02	174.32	174.96
Nb93	46.18	46.14	46.1	469.72	468.36	470.93	18.47	18.49	18.75
Cs133	32.15	32.71	32.54	312.52	315.05	313.08	0.103	0.102	0.09
Ba137	70.13	70.49	69.53	438.57	439.5	436.23	132.57	132.14	135.86
La139	40.46	40.35	40.31	408.94	408.28	408.5	15.81	15.67	15.28
Ce140	41.88	41.82	41.39	421.3	420.43	420.36	37.04	37.87	37.52
Pr141	46.37	46.72	46.57	481.43	484.68	481.45	5.22	5.28	5.3
Nd146	45.41	46.16	44.8	466.82	464.13	469.1	24.36	26.18	25.03
Sm147	47.86	47.61	47.91	494.17	494.53	494.29	6.61	6.12	6.01
Eu153	40.82	41.21	41.45	419.04	420.04	422.25	2.05	2.08	2.07
Gd157	50.59	50.83	51.07	528.51	531.76	533.17	6.31	6.23	6.49
Tb159	49.44	50.48	50.44	517.27	520.13	526.24	0.919	0.915	0.981
Dy163	52.5	54.08	54.51	552.62	552.27	555.15	5.43	5.58	5.44
Ho165	51.32	51.53	52.26	531.51	534.9	534.03	0.982	0.957	1.006

Er166	40.3	39.89	39.37	615.42	617.21	622.08	2.55	2.48	2.58
Tm169	51.89	53.22	52.21	541.68	541.42	544.72	0.356	0.326	0.334
Yb171	52.86	55.32	53.82	555.62	555.67	558.67	2.19	1.97	2.07
Lu175	54.95	55.62	55.33	563.43	563.89	565.87	0.276	0.304	0.292
Hf178	41.34	41.45	41.5	421.75	421.91	423.71	4.29	4.44	4.58
Ta181	44.97	45.46	44.96	455.61	456.09	461.01	1.175	1.135	1.13
Pb206	52.17	51.59	51.79	408.84	409.74	408.58	1.9	1.84	1.87
Pb207	52.83	50.86	51.4	404.77	409.29	404.09	2.33	1.78	1.86
Pb208	52.33	51.36	52.54	404.83	408.39	404.6	1.91	1.85	2.01
Th232	43.89	46.59	42.97	410.36	410.3	414.36	1.262	1.3	1.207
U238	41.58	41.11	41.77	420.7	420.87	420.55	0.456	0.418	0.444

Element	16-4-02_DT081105C-1	17-1-01_DT072609-1	19-3-01_22KK-BAt-02b-1	19-4-02_22KK-BAt-02b-1	19-6-03_DT092706C-1	20-4-01_DT091407A-1
Na23	27849.89	35493.82	38290.48	39644.95	37600.34	24748.57
Mg25	1024.79	3163.39	6626.12	4257.48	5522.33	851.75
Al27	67426.49	79758.02	81610.4	82139.65	82563.05	66103.37
Si29	343326.06	299740.13	313920.44	323082.31	289578.44	353706.22
K39	28778.6	35778.24	32917.99	36193.56	30512.79	34499.2
Ca43	6996.53	10971.77	17218.39	13345.38	20630.41	6209.13
Sc45	2.23	8.75	9.3	8.36	7.15	2.75
Ti47	1120.59	4905.51	6710.93	4976.37	4107.59	1200.87
Cr53	<0.00	<0.00	<0.00	<0.00	<0.00	<0.00
Fe57	7604.58	27673.71	40317.35	28088.9	26342.88	7763.96
Ni60	<0.76	0.91	3.24	<0.74	1.19	<1.21
Rb85	75.4	93.91	81.85	93.56	73.49	77.6
Sr88	135.72	195.66	340.41	245.02	538.27	108.77
Y89	10.76	39.89	34.33	37.5	34.05	12.12
Zr90	123.29	474.87	436.79	461.93	389.13	131.39
Nb93	6.21	25.44	24.66	26.5	21.72	6.37
Cs133	3.42	2.41	2.38	2.5	2.05	3.42
Ba137	813.37	923.65	918.41	991.43	945.07	849.69
La139	21.35	41.02	36.53	38.8	37.14	20.82
Ce140	39.96	82.58	74.82	78.74	76.41	40.37
Pr141	4.21	9.93	8.9	9.33	9.04	4.36
Nd146	14.35	38.06	33.74	35.87	34.52	14.72
Sm147	2.14	7.45	6.99	6.95	7.39	2.21
Eu153	0.41	1.037	1.241	1.258	1.37	0.392
Gd157	1.93	6.87	5.75	6.36	5.96	1.45
Tb159	0.282	1.037	0.87	1.04	0.972	0.313
Dy163	1.47	6.67	5.61	6.29	5.76	1.54

Ho165	0.361	1.517	1.248	1.388	1.139	0.335
Er166	0.92	4.41	3.5	4.25	3.6	1.22
Tm169	0.193	0.681	0.522	0.577	0.525	0.232
Yb171	1.39	4.55	3.97	4.11	3.98	1.84
Lu175	0.214	0.682	0.59	0.67	0.563	0.219
Hf178	3.47	10.91	9.61	10.86	8.68	4.46
Ta181	0.655	1.52	1.471	1.655	1.448	0.671
Pb206	14.06	18.06	14.38	14.61	13.41	15.09
Pb207	15.37	16.49	15.2	15.92	14.14	15.96
Pb208	14.78	17.59	14.9	15.41	13.94	16.06
Th232	11.45	13.08	11.7	12.45	10.54	12
U238	3.91	5.07	4.7	5.2	4.14	4

Element	20-4-02_DT091407A-1	20-4-03_DT091407A-1	21-2-01_DT072306B-1	21-2-02_DT072306B-1	25-2-01_HLGPush1_BA_A-1	25-6-02_HLGPush1_BA_A-1
Na23	26582.8	27412.14	34908.15	37977.25	38455.84	39810.19
Mg25	1005.41	1009.56	3338.24	5070.01	5286.99	3905.6
Al27	65732.89	65679.96	80075.58	81398.7	89496.23	91189.84
Si29	342168.31	356418.66	271143.34	311979.97	283061.63	294042.09
K39	29028.95	29591.26	26186.71	36013.62	29088.47	29669.99
Ca43	7024.72	6752.75	22458.35	14636.6	23450.05	24232.95
Sc45	2.51	3.12	6.17	8.7	7.28	6.7
Ti47	1205.24	1224.66	3677.69	5337.33	4272.54	3923.24
Cr53	<0.00	<0.00	<0.00	<0.00	<0.00	<0.00
Fe57	7940.16	8209.21	22842.19	31996.32	25642.61	23154.92
Ni60	<1.13	<1.54	<0.81	<0.63	0.91	1.31
Rb85	73.12	73.8	65.48	91.68	68.04	68.87
Sr88	130.25	131.05	599.94	256.35	681.06	788.7
Y89	11.87	11.53	25.78	37.99	31.48	30.01
Zr90	134.96	134.84	315.48	453.35	371.6	362.12
Nb93	6.15	5.9	18.15	25.07	20.48	20.1
Cs133	3.28	3.14	1.8	2.53	1.78	1.857
Ba137	807.94	804.24	792.34	990.69	974.76	990.37
La139	20.65	21.09	28.61	39.88	35.1	32.68
Ce140	39.36	39.38	58.03	82.77	69.98	66.99
Pr141	4.02	3.85	6.93	9.91	8.31	7.88
Nd146	13.95	14.64	25.23	36.8	33.64	30.75
Sm147	2.35	2.45	4.94	7.47	6.15	6.12
Eu153	0.421	0.367	1.128	1.256	1.25	1.329
Gd157	1.78	1.42	4.45	6.29	6.01	4.73
Tb159	0.264	0.296	0.746	1.009	0.818	0.765
Dy163	1.51	1.36	4.46	6.31	5.58	4.67

Ho165	0.41	0.429	0.929	1.376	1.143	1.031
Er166	1.29	1.02	2.64	4	3.18	2.93
Tm169	0.223	0.159	0.381	0.578	0.439	0.453
Yb171	1.18	1.49	3.31	4.22	3.48	3.24
Lu175	0.26	0.207	0.362	0.657	0.575	0.494
Hf178	3.86	3.64	7.13	10.36	8.4	8.17
Ta181	0.585	0.631	1.018	1.538	1.118	1.182
Pb206	15.01	14.94	12.09	16.06	13.02	12.6
Pb207	14.79	15.6	11.86	17.45	13.33	13.15
Pb208	15.69	16.16	11.84	16.55	13.36	13.41
Th232	11.1	10.94	8.21	12.46	9.39	9.39
U238	3.73	4	3.7	4.95	3.8	3.71

Element	25-6-03_HLGPush1_BA_A-1	25-3-01_HLGPush1_BA_B-1	25-3-02_HLGPush1_BA_B-1	25-4-03_HLGPush1_BA_C-1	25-4-04_HLGPush1_BA_C-1	25-5-05_HLGPush1_BA_C-1
Na23	40292.75	36712.49	37986.56	39455.78	42960.32	38297.74
Mg25	6716.27	6634.23	3125.06	3891.91	10185.77	3989.96
Al27	91772.01	81769.18	79281.7	86109.03	93571.45	95053.35
Si29	330360	302829.25	304172.28	296265.91	337200	263144
K39	38708.91	35916.16	38827.85	31786.05	33169.76	21836.46
Ca43	19009.59	15154.51	11151.95	19294.55	23427.35	31159.42
Sc45	8.46	7.4	7.16	6.45	7.74	5.11
Ti47	5291.59	4737.34	5028.72	5429.11	4615.09	3315.03
Cr53	<0.00	<0.00	<0.00	<0.00	<0.00	<0.00
Fe57	30946.5	29763.99	24679.86	31798.38	35345.63	22519.34
Ni60	1.96	1.93	1.15	2.23	3.82	<0.65
Rb85	93.23	85.63	98.79	75.52	79.34	48.21
Sr88	508.79	367.06	232.14	560.56	730.02	1141.78
Y89	38.84	34.86	32.92	29.84	32.48	20.1
Zr90	491.65	442.4	425.58	398.65	401.63	251.23
Nb93	26.68	24.59	24.9	22.68	23.23	14.28
Cs133	2.55	2.38	2.55	2.06	2.13	1.455
Ba137	1045.54	959.2	1034.68	969.4	1061.93	842.36
La139	41.85	37.71	36.54	33.71	36.46	24.41
Ce140	86.11	76.25	74.99	68.36	75.33	49.24
Pr141	10.29	9.32	8.94	7.91	9.1	5.72
Nd146	39.17	34.9	32.28	29.28	36.6	21.24
Sm147	6.99	7.03	6.1	5.76	6.12	4.2
Eu153	1.407	1.232	1.095	1.193	1.28	1.247
Gd157	6.69	5.61	5.98	5.16	5.22	3.58
Tb159	0.984	0.915	0.847	0.733	0.799	0.531
Dy163	6.37	5.62	5.24	4.91	5.43	2.99

Ho165	1.282	1.176	1.113	0.953	1.07	0.7
Er166	3.94	3.57	3.06	3.05	3.2	1.87
Tm169	0.602	0.549	0.449	0.502	0.542	0.319
Yb171	4.29	3.78	3.54	3.25	3.52	2.27
Lu175	0.704	0.62	0.499	0.523	0.473	0.318
Hf178	10.91	10.22	9.97	9.08	9.03	5.22
Ta181	1.617	1.475	1.415	1.326	1.28	0.827
Pb206	16.37	15.46	17.85	13.54	14.18	10.58
Pb207	16.05	15.24	18.17	14.54	14.55	10.44
Pb208	16.08	14.99	18.33	14.05	14.16	10.63
Th232	12.76	11.36	12.19	10.06	10.23	6.48
U238	4.93	4.49	4.73	4.13	4.2	2.6

Element	GSE-7	GSE-8	GSE-9	BHVO2-7	BHVO2-8	BHVO2-9	GSD-7	GSD-8	GSD-9
Na23	30586.92	30276.84	30551.62	17611.48	17604.42	18169.31	28421.74	28238.79	28361.04
Mg25	21380.29	21308.87	21381.51	45283.25	44740.91	45583.32	21596.48	21435.6	21650.45
Al27	70912.99	70912.98	70912.98	71970.98	71970.98	71970.98	72499.98	72499.98	72499.98
Si29	245458.11	243801.13	245838.94	235738.63	236218.19	242629.11	245780.48	244799.39	246543.95
K39	21705.96	21483.73	21689.04	4237.96	4255.9	4390.54	25163.12	25116.6	25026.96
Ca43	52243.86	52355.28	52535.64	82096.22	82733.95	80429.59	51092.29	51644.25	51471.11
Sc45	539.86	535.15	542.17	32.92	33.46	33.32	52.33	53.14	53.08
Ti47	444.99	447.47	456.27	16439.26	16480.85	16400.37	7787.44	7791.08	7771.71
Cr53	<0.00	<0.00	<0.00	<0.00	<0.00	<0.00	<0.00	<0.00	<0.00
Fe57	101122.34	100142.63	100238.36	92527.18	93191.94	96392.48	103125.45	103508.06	103329.76
Ni60	423.47	420.62	423.04	120.66	120.61	124.29	55.68	57.86	55.6
Rb85	369.26	366.16	368.83	9.28	9.24	9.62	37.39	38.03	38.24
Sr88	450.43	448.24	449.87	390.42	387.63	388.72	69.27	69.22	69.29
Y89	456.46	452.64	458.04	26.06	26.49	26.38	45.01	45.01	44.64
Zr90	431.21	431.81	428.86	171.44	172.55	172.07	44.56	44.6	44.48
Nb93	464.87	463.37	465.5	18.32	18.57	18.24	45.97	46.28	45.56
Cs133	313.05	309.27	313.02	0.108	0.128	0.092	31.96	32.46	32.24
Ba137	429.57	431.82	434.41	131.64	130.23	130.84	68.16	69.88	69.33
La139	402.18	399.78	401.64	15.25	15.26	15.23	39.96	40.25	39.32
Ce140	412.48	413.05	414.86	37.16	36.99	37.24	41.07	41.08	40.82
Pr141	471.3	470.79	473.71	5.29	5.21	5.05	45.47	46.31	45.92
Nd146	457.7	453.1	456.38	23.79	23.29	24.13	44.77	44.28	44.96
Sm147	481.07	485.55	486.48	5.81	6.11	6.27	46.91	48.1	47.51
Eu153	409.06	411.76	415.01	1.89	2.09	2.02	40.89	40.32	40.71
Gd157	518.61	519.54	521.93	5.9	6.14	6.12	49.73	49.84	50.19
Tb159	508.5	511.65	514.62	0.923	0.897	0.906	49.34	49.76	49.01
Dy163	540.65	543.86	546.11	5.35	5.09	5	52.83	53.29	52.79
Ho165	521.96	524.45	525.81	1.034	0.909	0.992	50.92	50.75	50.82

Er166	601.28	602.35	609.23	2.42	2.55	2.65	39.1	39.83	39.53
Tm169	533.22	532.76	537.41	0.356	0.31	0.313	51.54	51.95	51.5
Yb171	544.38	539.16	549.4	2.05	1.87	1.98	53.02	53.58	52.84
Lu175	546.31	550.34	553	0.306	0.269	0.28	54.61	54.09	54.63
Hf178	412.83	410.23	416.69	4.61	4.4	4.28	40.59	41.16	40.26
Ta181	443.6	443.18	447.94	1.075	1.13	1.177	44.45	43.56	44.24
Pb206	401.5	397.83	402.99	1.82	1.86	1.77	49.89	50.95	51.89
Pb207	395.02	391.55	394.93	1.98	1.85	2.06	50.37	50.66	51.93
Pb208	396.76	393.69	400.19	1.93	1.96	1.89	50.91	50.83	50.72
Th232	394.98	393.58	395.37	1.27	1.26	1.22	42.13	42.81	44.84
U238	410.49	408.37	414.31	0.417	0.415	0.417	40.06	40.07	40.51